ARTICLE

A TNF-IL-1 circuit controls *Yersinia* within intestinal pyogranulomas

Rina Matsuda[1]*, Daniel Sorobetea[1]*, Jenna Zhang[2]*, Stefan T. Peterson[1], James P. Grayczyk[1], Winslow Yost[1], Nicolai Apenes[1], Maria E. Kovalik[1], Beatrice Herrmann[1], Rosemary J. O'Neill[1], Andrea C. Bohrer[3], Matthew Lanza[1], Charles-Antoine Assenmacher[1], Katrin D. Mayer-Barber[3], Sunny Shin[2], and Igor E. Brodsky[1]

Tumor necrosis factor (TNF) is a pleiotropic inflammatory cytokine that mediates antimicrobial defense and granuloma formation in response to infection by numerous pathogens. We previously reported that *Yersinia pseudotuberculosis* colonizes the intestinal mucosa and induces the recruitment of neutrophils and inflammatory monocytes into organized immune structures termed pyogranulomas (PG) that control *Yersinia* infection. Inflammatory monocytes are essential for the control and clearance of *Yersinia* within intestinal PG, but how monocytes mediate *Yersinia* restriction is poorly understood. Here, we demonstrate that TNF signaling in monocytes is required for bacterial containment following enteric *Yersinia* infection. We further show that monocyte-intrinsic TNFR1 signaling drives the production of monocyte-derived interleukin-1 (IL-1), which signals through IL-1 receptors on non-hematopoietic cells to enable PG-mediated control of intestinal *Yersinia* infection. Altogether, our work reveals a monocyte-intrinsic TNF-IL-1 collaborative inflammatory circuit that restricts intestinal *Yersinia* infection.

Introduction

Granulomas form in response to a wide variety of infections, acting as barriers to pathogen dissemination (Petersen and Smith, 2013; Pagán and Ramakrishnan, 2018). Although generally considered protective, granulomas can also provide a replicative niche from which pathogens can spread, such as in immune-compromised patients who experience reactivation of latent *Mycobacterium tuberculosis* (Davis and Ramakrishnan, 2009; Diedrich et al., 2016). Moreover, pathogens within granulomas often exist in an antibiotic-resistant state and can pose a significant therapeutic challenge (Adams et al., 2011). Granulomas thus represent a localized niche where pathogens can be contained but can also resist immune clearance. Understanding how immune cells communicate within chronic granulomatous lesions to control pathogens remains an important question that could enable the development of immunomodulatory treatments against infectious agents that persist within this niche.

Pyogranulomas and pyogranulomatous lesions (PGs) are a subset of chronic granulomatous inflammation characterized by a predominance of neutrophils and macrophages, often in combination with plasma cells and giant cells (Raskin, 2010). The enteropathogenic *Yersiniae*, which include *Yersinia pseudotuberculosis* (*Yp*) and *Yersinia enterocolitica*, colonize the intestinal mucosa and lymphoid tissues of both mice and humans, triggering formation of PGs that are composed of extracellular bacterial colonies in close association with neutrophils, bordered closely by monocytes and macrophages (El-Maraghi and Mair, 1979; Lamps et al., 2001; Kojima et al., 2007; Rohena et al., 2014; Peterson et al., 2017; Zhang et al., 2018; Sorobetea et al., 2023).

We previously demonstrated that organized PGs, characterized by central cores of cell debris surrounded by dense cuffs of neutrophils and epithelioid macrophages, form by 5 days after *Yp* infection within the mesenteric lymph nodes (MLN) (Peterson et al., 2017). We recently also described organized

---

[1]Department of Pathobiology, School of Veterinary Medicine, University of Pennsylvania, Philadelphia, PA, USA; [2]Department of Microbiology, Perelman School of Medicine, University of Pennsylvania, Philadelphia, PA, USA; [3]Inflammation and Innate Immunity Unit, Laboratory of Clinical Immunology and Microbiology, National Institute of Allergy and Infectious Diseases, National Institutes of Health, Bethesda, MD, USA.

*R. Matsuda, D. Sorobetea, and J. Zhang contributed equally to this paper. Correspondence to Igor E. Brodsky: ibrodsky@vet.upenn.edu; Sunny Shin: sunshin@pennmedicine.upenn.edu

R. Matsuda's current affiliation is Department of Molecular Virology and Microbiology, Baylor College of Medicine, Houston, TX, USA. J.P. Grayczyk's current affiliation is Oncology Discovery, AbbVie, Inc., North Chicago, IL, USA. M. Lanza's current affiliation is Penn State Health Milton S Hershey Medical Center, Penn State College of Medicine, Hershey, PA, USA.

PGs containing viable bacteria, a central neutrophil core, inflammatory monocytes, and epithelioid macrophages along the length of the gastrointestinal tract following oral *Yp* infection (Sorobetea et al., 2023). PGs formed in response to the activity of *Yp* outer proteins (Yops), which are injected into host cells through the *Yp* type III secretion system and block essential antimicrobial functions (Atkinson and Williams, 2016; Bliska et al., 2021; Sorobetea et al., 2023). We further demonstrated that inflammatory monocytes were critical for the maintenance of organized PGs and enabling neutrophils to overcome the activity of *Yp* virulence factors that block host phagocytosis and oxidative burst (Sorobetea et al., 2023). However, the mechanisms by which inflammatory monocytes mediate anti-*Yp* host defense are unclear.

Tumor necrosis factor (TNF) is a pleiotropic inflammatory cytokine associated with protection during infectious granulomatous disease, notably tuberculosis (Kindler et al., 1989; Flynn et al., 1995; Bean et al., 1999; Roach et al., 2002; Algood et al., 2005; Chakravarty et al., 2008; Clay et al., 2008; Lin et al., 2010). While the role of TNF in maintaining intact granulomas is well-appreciated, its precise cellular targets and mechanisms of action remain elusive due to the broad expression of its main receptor, TNFR1, and its numerous downstream signaling functions, including cell-extrinsic apoptosis, promotion of cell survival, and control of proinflammatory gene expression (Chen and Goeddel, 2002; Takeda and Akira, 2004; Kusnadi et al., 2019). TNF plays a critical role in protection against infection by intracellular pathogens, as the extensive clinical use of anti-TNF blockade in the setting of autoinflammatory disease is associated with an increased risk of severe infections (Ali et al., 2013; Kusnadi et al., 2019).

Although *Yp* is primarily an extracellular pathogen, TNF is required for host protection against *Yp* (Autenrieth and Heesemann, 1992; Parent et al., 2006; Peterson et al., 2016). However, the mechanisms by which TNF controls *Yp* infection are not completely understood. Here, we demonstrate that monocytes serve as an essential cellular source of TNF during *Yp* infection. We find that signaling through both the TNF and IL-1 receptors is required to control *Yp* replication in PGs. Intriguingly, monocyte-intrinsic TNF production and receptor signaling are required for monocytes within PGs to produce IL-1. IL-1R signaling is required for the production of the chemokine CXCL1, and we further find that IL-1 receptor is required on non-hematopoietic cells to mediate control of intestinal *Yp* infection. Altogether, our study demonstrates that a monocyte-driven TNF-IL-1 feedforward circuit mediates the control of *Yp* infection within systemic and intestinal sites.

Results

TNFR1 is required for organized PG formation and *Yp* control
We recently identified the formation of PGs in the murine intestinal mucosa during acute *Yp* infection, wherein inflammatory monocytes were required for neutrophil activation, maintenance of organized PG architecture, and bacterial clearance (Sorobetea et al., 2023). TNF is critical for granuloma maintenance and bacterial control in the lung during tuberculosis infection

(Kindler et al., 1989; Flynn et al., 1995; Bean et al., 1999; Roach et al., 2002; Algood et al., 2005; Chakravarty et al., 2008; Clay et al., 2008; Lin et al., 2010), and we previously reported that TNFR1 is required to control systemic bacterial burdens following oral *Yp* infection (Peterson et al., 2016). Notably, while *Tnfr1*$^{-/-}$ mice formed similar numbers of macroscopic intestinal lesions as wild-type (WT) mice at day 5 after infection (Fig. S1 A), histopathologic analyses revealed that intestinal lesions in *Tnfr1*$^{-/-}$ mice were strikingly similar to lesions that we recently described in *Yp*-infected CCR2-deficient mice lacking circulating monocytes (Sorobetea et al., 2023) (Fig. 1 A). In contrast to WT PG, which had robust immune cell aggregation and a small central *Yp* microcolony, *Tnfr1*$^{-/-}$ intestinal lesions contained an area of central necrosis surrounded by a greatly expanded *Yp* colony, ringed by limited immune cell infiltrates (Fig. 1, A and B). In line with these histopathological findings, bacterial burdens in both PG-containing (PG$^+$) intestinal punch biopsies and adjacent non-PG (PG$^-$) biopsies were elevated in *Tnfr1*$^{-/-}$ mice (Fig. 1 C). Furthermore, *Tnfr1*$^{-/-}$ lesions contained fewer monocytes, macrophages, and neutrophils, as determined by flow cytometry (Fig. 1 D and Fig. S1, B and C). In line with these findings, whole-mount immunofluorescence microscopy revealed that in contrast to WT PG, where *Yp* bacteria are entirely contained within the CD11b$^+$ and Ly-6G$^+$ myeloid cell infiltrate, *Tnfr1*$^{-/-}$ PG had limited recruitment of CD11b$^+$ myeloid cells or Ly-6G$^+$ neutrophils and were unable to contain the dramatically expanded bacterial colony, similar to PG we previously described in CCR2-deficient animals (Sorobetea et al., 2023) (Fig. 1 E and Fig. S1 D). Surface expression of the integrin CD11b, a marker of neutrophil activation (Borjesson et al., 2002; Mann and Chung, 2006; Yoon et al., 2007), was also significantly reduced in PG of *Tnfr1*$^{-/-}$ mice compared with WT controls (Fig. 1 F), suggesting a defect in neutrophil activation in the absence of TNFR1 signaling, consistent with our recent finding that monocytes are required for maximal PG neutrophil activation (Sorobetea et al., 2023). Also consistent with our previous findings (Peterson et al., 2016), *Tnfr1*$^{-/-}$ mice exhibited elevated bacterial burdens in the spleen and liver (Fig. 1 G). Moreover, *Tnfr1*$^{-/-}$ mice succumbed to infection around day 8, while most WT mice survived (Fig. 1 H). Notably, while TNFR2 can also signal in response to TNF, TNFR2-deficient mice generally had no defect in intestinal or systemic control of *Yp* infection, with the exception of the liver, which showed only a relatively small increase in bacterial burdens at day 5 after infection (Fig. S1, E and F). Overall, these data suggest that signaling through TNFR1 rather than TNFR2 limits necrotic core formation in PGs during *Yp* infection and controls bacterial growth.

TNFR1 signaling can enhance the ability of both hematopoietic (immune) and non-hematopoietic (stromal and epithelial) cells to control pathogens (Flynn et al., 1995; Bean et al., 1999; Clay et al., 2008; Peterson et al., 2016; Pham et al., 2020). To test which compartment requires TNFR1 signaling to control *Yp*, we generated bone marrow (BM) chimeras in which TNFR1 expression was ablated in either the hematopoietic or non-hematopoietic compartment (Fig. S1 G). Mice lacking TNFR1 in either the hematopoietic or non-hematopoietic compartment
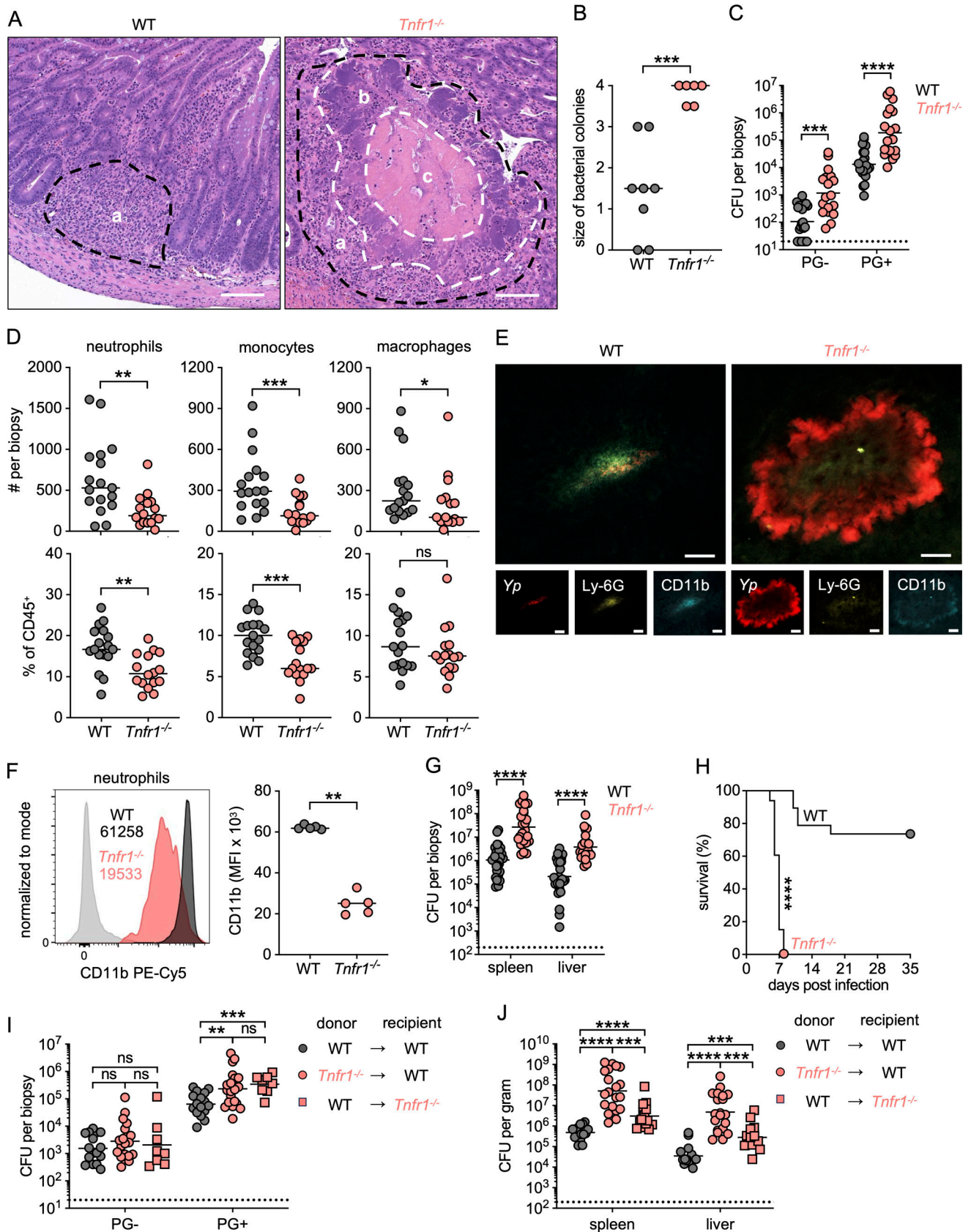
Figure 1. **TNFR1 is required for organized PG formation and *Yp* control. (A)** H&E-stained paraffin-embedded small intestinal sections from *Yp*-infected WT (left) and *Tnfr1⁻/⁻* (right) mice at day 5 after infection; a (black dashed lines) = immune cell infiltrate, b = bacterial colony, and c = necrosis. White dashed lines delineate the edges of central necrosis and extracellular colonies. Images representative of two independent experiments. Scale bars = 100 µm.

(B) Histopathological scores of small intestinal tissue from *Yp*-infected WT and *Tnfr1⁻/⁻* mice at day 5 after infection. Each mouse was scored between 0 and 4 (minimal to extensive) for the size of the bacterial colony. Each circle represents one mouse. Lines represent the median. Pooled data from two independent experiments. **(C)** Bacterial burdens in small intestinal PG⁻ and PG⁺ tissue isolated on day 5 after infection. Each circle represents the mean CFU of three to five pooled punch biopsies from one mouse. Lines represent the geometric mean. Pooled data from three independent experiments. **(D)** Total numbers (top) and frequencies (bottom) of neutrophils, monocytes, and macrophages in PG⁺ small intestinal tissue isolated 5 days after infection. Each circle represents the mean of 3–20 pooled punch biopsies from one mouse. Lines represent the median. Pooled data from three independent experiments. **(E)** Fluorescently labeled whole-mount small intestinal PG⁺ tissue from *Yp*-infected WT (left) and *Tnfr1⁻/⁻* (right) mice at day 5 after infection. Red (*Yp*-mCherry), yellow (Ly-6G-AF647), and blue (CD11b-AF700). Scale bars = 100 μm. Representative image of two independent experiments. **(F)** CD11b surface expression on neutrophils in PG⁺ tissue at day 5 after infection. Each circle represents the mean of 3–10 pooled punch biopsies from one mouse. Lines represent the median. Data are representative of three independent experiments. **(G)** Bacterial burdens in indicated organs at day 5 after infection. Each circle represents one mouse. Lines represent the geometric mean. Pooled data from four independent experiments. **(H)** Survival of infected WT (*n* = 9) and *Tnfr1⁻/⁻* (*n* = 21) mice. Pooled data from two independent experiments. **(I)** Bacterial burdens in small intestinal PG⁻ and PG⁺ tissue at day 5 after infection of indicated chimeric mice. Each symbol represents the mean *Yp* CFU of three to five pooled punch biopsies from one mouse. Lines represent the geometric mean. Pooled data from two independent experiments. **(J)** Bacterial burdens in indicated organs at day 5 after infection of indicated chimeric mice. Each symbol represents one mouse. Lines represent the geometric mean. Pooled data from two independent experiments. Statistical analysis by Mann–Whitney U test (B–D, F, and G), Mantel–Cox test (H), and Kruskal–Wallis test with Dunn's multiple comparisons correction (I and J). *P < 0.05, **P < 0.01, ***P < 0.001, ****P < 0.0001, ns = not significant.

had elevated bacterial burdens within PG compared with WT control chimeras, indicating that TNFR1 signaling is required non-redundantly in both hematopoietic and non-hematopoietic cells to mediate control of intestinal *Yp* (Fig. 1 I). In contrast, mice lacking TNFR1 in hematopoietic cells had highly elevated bacterial burdens in the systemic tissues, while mice lacking TNFR1 in non-hematopoietic cells had a significant but smaller increase in systemic bacterial burdens compared with WT controls (Fig. 1 J). Taken together, these results demonstrate that TNFR1 signaling in both hematopoietic and non-hematopoietic cells contribute to bacterial control in the intestine, while TNFR1 signaling in hematopoietic cells plays a dominant role in bacterial control in systemic tissues during acute *Yp* infection.

Autocrine TNF signaling in monocytes is required for control of *Yp*

TNF receptor expression is widespread in both hematopoietic and non-hematopoietic cells, raising the question of which cells require TNF signaling for the control of *Yp* infection. CCR2-deficient mice lacking circulating monocytes fail to form functional intestinal PG, are unable to control *Yp* burdens, and rapidly succumb to infection (Sorobetea et al., 2023). Given the similar outcomes of infection and histopathological appearance of PG in TNFR1- and CCR2-deficient mice, we sought to test the hypothesis that TNF is produced and/or detected by monocytes. We generated mice in which TNFR1 was specifically deleted on inflammatory monocytes by means of mixed BM chimera where irradiated WT recipient mice were reconstituted with a 1:1 ratio of *Ccr2^gfp/gfp^*:*Tnfr1⁻/⁻* BM cells. Since CCR2-deficient cells are unable to egress from the BM to enter circulation (Serbina and Pamer, 2006), this approach generates mice in which circulating CCR2⁺ monocytes are derived only from the *Tnfr1⁻/⁻* cells, whereas other hematopoietic cell types arise from both genotypes and are thus sufficient for TNFR1 signaling (Fig. 2 A and Fig. S2 A). Intriguingly, compared with WT chimeric mice, mice lacking TNFR1 specifically on CCR2⁺ monocytes formed intestinal PG lesions with expanded bacterial colonies and had elevated bacterial burdens in PG⁻ and systemic tissues, indicating a failure to control *Yp* infection and largely recapitulating the phenotype of mice lacking CCR2 in the entire hematopoietic system (Fig. 2, B–D). Despite apparent gross histological differences,

bulk PG bacterial burdens as measured by colony-forming units (CFUs) were comparable across chimeric genotypes, potentially due to the general increased susceptibility of irradiated chimeric mice to infection (Fig. 2 C). Importantly, the defect in bacterial control was not due to the absence of TNFR1 expression on 50% of immune cells, as mixed chimeras from *Tnfr1⁻/⁻*:WT chimeric mice still had significantly lower bacterial burdens relative to *Tnfr1⁻/⁻*:*Ccr2^gfp/gfp^* mice, notably in systemic tissues (Fig. S2, B–D). Notably, mice lacking TNFR1 expression on all hematopoietic cells had significantly higher burdens than mice lacking TNFR1 on monocytes alone (Fig. S2 C). Altogether, these data suggest that while TNFR1 has additional important roles in other cell types beyond monocytes, TNFR1 signaling in monocytes is nonetheless essential for their protective role against *Yp* infection.

Multiple immune cell types produce TNF in response to inflammatory signals, including monocytes, which are a major source of TNF during *Yp* infection (Peterson et al., 2017). To test whether monocyte-derived TNF is important for control of *Yp* infection, we reconstituted irradiated WT recipient mice with a 1:1 ratio of *Ccr2^gfp/gfp^*:*Tnf⁻/⁻* BM cells, thereby generating cohorts of mice in which circulating CCR2⁺ monocytes lacked the ability to produce TNF, with other hematopoietic cell types being comprised of a 1:1 mixture of WT and *Tnf⁻/⁻* cells (Fig. S2 E). Strikingly, mice lacking TNF specifically in monocytes failed to control *Yp* infection in the spleen and liver and had bacterial burdens comparable with mice lacking TNF production in all hematopoietic cells (Fig. 2, E and F). Altogether, our findings demonstrate that autocrine TNF signaling in monocytes is required to control enteric *Yp* infection.

TNFR1 signaling in monocytes controls *Yp* independently of RIPK1 kinase–induced cell death

TNFR1 can mediate inflammatory gene expression or promote cell-extrinsic apoptosis in response to infection by pathogens, including *Yp* (Ea et al., 2006; Ofengeim and Yuan, 2013; Christofferson et al., 2014; Weinlich and Green, 2014; Peterson et al., 2016; Delanghe et al., 2020; Yeap and Chen, 2022). *Yp*-induced cell death is triggered by YopJ-mediated blockade of IκB kinase signaling and involves contributions from both TLR4/TRIF and TNFR1 signaling through the kinase activity of the
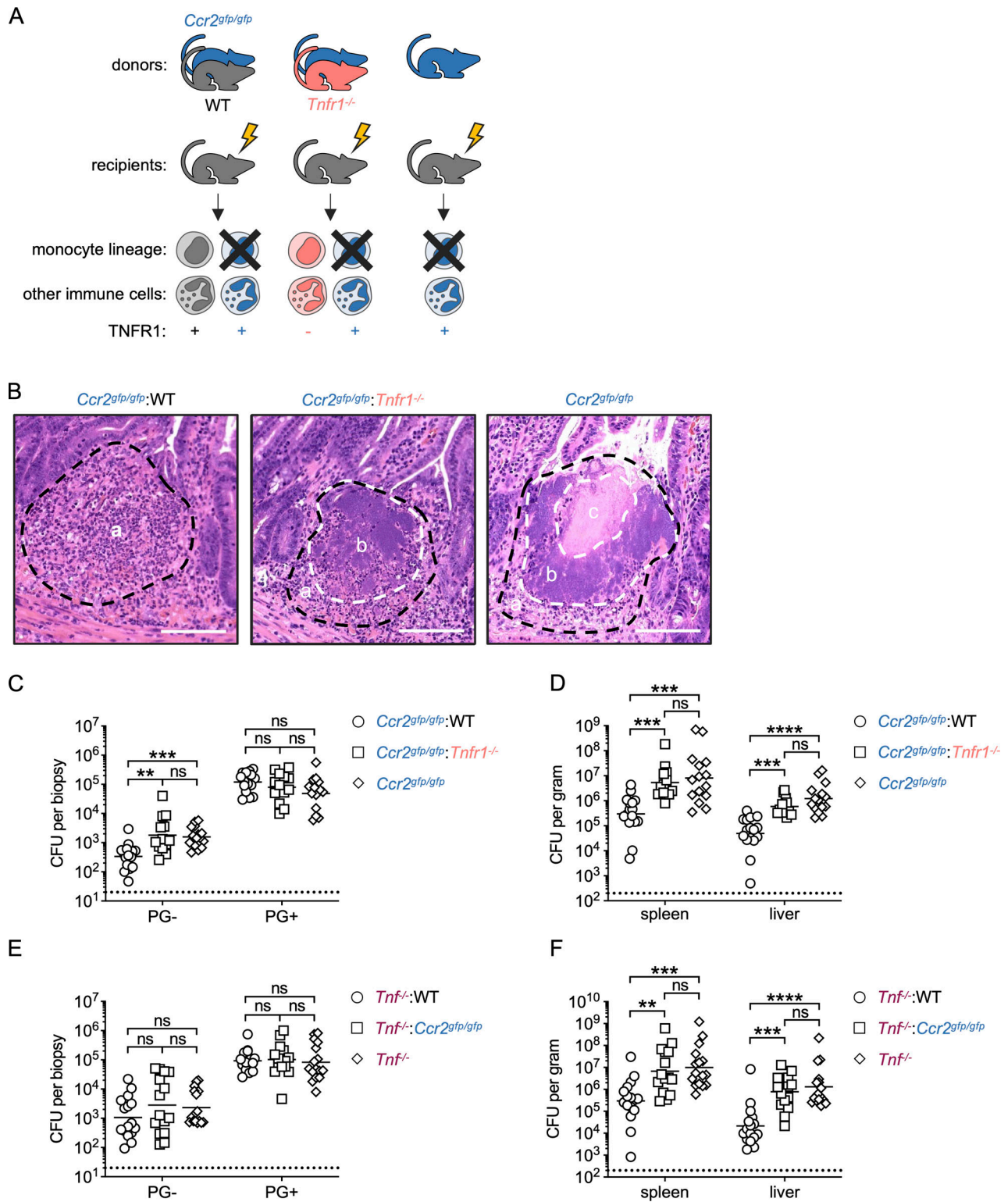
Figure 2. **Autocrine TNF signaling in monocytes is required for control of *Yp*. (A)** Schematic of mixed BM chimeras. Lethally irradiated WT mice reconstituted with BM cells from indicated donor mice yield either a TNFR1-sufficient immune system (left), an immune system in which all monocytes lack TNFR1 whereas half of the remaining immune cells are TNFR1-proficient (middle), or a TNFR1-sufficient immune system devoid of monocytes (right). **(B)** H&E-stained paraffin-embedded small intestinal sections from chimeric WT mice reconstituted with *Ccr2^gfp/gfp^* + WT (left), *Ccr2^gfp/gfp^* + *Tnfr1^−/−^* (middle), or *Ccr2^gfp/gfp^* (right) BM at day 5 after infection; a (black dashed lines) = immune cell infiltrate, b = bacterial colony, c = necrosis. White dashed lines delineate the edges of central necrosis and extracellular bacterial colonies. Scale bars = 100 μm. Images representative of two independent experiments. **(C)** Bacterial burdens in small intestinal PG− and PG+ tissue of chimeric WT mice reconstituted with either *Ccr2^gfp/gfp^*:WT (circles), *Ccr2^gfp/gfp^*:*Tnfr1^−/−^* (squares), or *Ccr2^gfp/gfp^* (diamonds) at day 5 after *Yp* infection. Each symbol represents one mouse. Lines represent the geometric mean. Pooled data from two independent experiments. **(D)** Bacterial burdens in indicated organs at day 5 after infection. Each symbol represents one mouse. Lines represent the geometric mean. Pooled data from

two independent experiments. **(E)** Bacterial burdens in small intestinal PG⁻ and PG⁺ tissue of chimeric WT mice reconstituted with either *Tnf*⁻/⁻:WT (circles), *Tnf*⁻/⁻:*Ccr2*^gfp/gfp^ (squares), or *Tnf*⁻/⁻ (diamonds) at day 5 after *Yp* infection. Each symbol represents one mouse. Lines represent the geometric mean. Pooled data from three independent experiments. **(F)** Bacterial burdens in indicated organs at day 5 after infection. Each symbol represents one mouse. Lines the represent geometric mean. Pooled data from three independent experiments. All statistical analyses by Kruskal–Wallis test with Dunn's multiple comparisons correction. **P < 0.01, ***P < 0.001, ****P < 0.0001, ns = not significant.

adapter RIPK1 (Monack et al., 1997; Palmer et al., 1998; Orth et al., 1999; Yoon et al., 2003; Mukherjee et al., 2006; Philip et al., 2014; Peterson et al., 2017). We previously demonstrated that mice lacking RIPK1 kinase activity (*Ripk1*^K45A^) in hematopoietic cells fail to form intact MLN PG and rapidly succumb to *Yp* infection (Peterson et al., 2017). Furthermore, activation of gasdermin D and gasdermin E in macrophages and neutrophils, respectively, downstream of RIPK1 kinase activity promotes control of *Yp* infection (Chen et al., 2021). We hypothesized that RIPK1 activation downstream of TNFR1 signaling in monocyte-lineage cells mediates control of *Yp* within intestinal PGs. Notably, *Ripk1*^K45A^ mice formed necrotic intestinal lesions and were deficient in restricting *Yp* burdens (Fig. 3, A and B), consistent with prior findings (Peterson et al., 2017). To test whether monocyte-intrinsic TNFR1 signaling promotes anti-*Yp* host defense through activation of RIPK1-induced monocyte cell death, we generated mixed BM chimeras in which irradiated WT recipient mice were reconstituted with a 1:1 ratio of *Ccr2*^gfp/gfp^: *Ripk1*^K45A^ BM cells. Reconstituted mice contained CCR2⁺ monocytes that lacked RIPK1 kinase activity, with other hematopoietic cells being equally reconstituted by both donor BM progenitors (Fig. S3, A and B). Surprisingly, monocyte-specific ablation of RIPK1 kinase activity did not impact the ability of mice to form intact intestinal PG or control enteric *Yp* infection (Fig. 3, C–E), indicating that RIPK1 kinase activity in monocytes is dispensable to control *Yp* infection downstream of TNF signaling. We previously found that the acute susceptibility of *Ripk1*^K45A^ mice is reversed in the setting of infection with YopJ-deficient bacteria, illustrating that RIPK1 kinase–induced cell death is necessary to counteract the blockade of immune signaling by YopJ (Peterson et al., 2017). However, *Tnfr1*⁻/⁻ mice still formed necrotic intestinal PG, failed to control bacterial burdens in systemic tissues, and succumbed to infection by YopJ-deficient bacteria (Fig. 3, F–H). Collectively, these data indicate that monocyte-dependent TNFR1 signaling mediates anti-*Yp* host defense via a mechanism distinct from YopJ-dependent, RIPK1-induced cell death.

We recently reported that intestinal PGs form in response to the activities of the *Yp* effectors YopE and YopH, and that monocytes counteract YopH-mediated blockade of innate immunity (Sorobetea et al., 2023). YopE and YopH both block phagocytosis and the oxidative burst through actin cytoskeleton disruption (Rosqvist et al., 1988, 1991; Bliska et al., 1991; Galyov et al., 1993; Bliska and Black, 1995; Green et al., 1995; Mecsas et al., 1998; Black and Bliska, 2000; Grosdent et al., 2002; Taheri et al., 2016). However, whether TNFR1 is required to overcome the immune blockade posed by YopE and YopH is unknown. Strikingly, TNFR1-deficient mice largely survived infection with *yopEH* mutant *Yp* (Fig. 3 I), indicating that TNFR1 signaling counteracts the activity of YopE and YopH. However, in contrast to our previous findings with CCR2-deficient mice

(Sorobetea et al., 2023), *Tnfr1*⁻/⁻ mice were not able to control either single *Yp* mutant, although there was a modest but significant decrease in mortality in response to infection with *yopH* mutant bacteria (Fig. S3 C). Together, these findings demonstrate that TNFR1 signaling controls enteric *Yp* infection by counteracting the virulence activities of YopE and YopH.

Cell-intrinsic TNFR1 signaling is required for maximal IL-1 production within intestinal PGs during *Yp* infection

Our findings collectively indicate that monocyte-intrinsic TNFR1 signaling promotes intestinal PG formation and control of *Yp* infection via RIPK1 kinase–independent mechanisms. We therefore considered that TNFR1 signaling in monocytes contributes to the control of *Yp* infection by promoting inflammatory cytokine production. Multiplex cytokine profiling of intestinal PG⁺ and PG⁻ from mixed BM chimeric mice with monocyte-intrinsic TNFR1 deficiency revealed that IL-1α levels were significantly decreased in the PG lesions of these mice (Fig. 4 A), in contrast to other proinflammatory cytokines such as IL-6 (Fig. S4 A). Neither IL-1α nor IL-1β were detected in the sera of these mice at day 5 after *Yp* infection, suggesting that IL-1 production in response to TNFR1 signaling is localized to intestinal PG (Fig. S4 B). Since TNFR1 expression on monocytes is required for restriction of bacterial burdens, we hypothesized that TNFR1 signaling promotes monocyte production of IL-1 within intestinal PG. Indeed, *Tnfr1*⁻/⁻ monocytes and neutrophils exhibited reduced levels of IL-1α and IL-1β expression as determined by intracellular cytokine staining, indicating that TNFR1 signaling is necessary for maximal IL-1 production in both monocytes and neutrophils within intestinal PG (Fig. 4 B). To test whether TNFR1 is required in a cell-intrinsic or -extrinsic manner to promote IL-1 expression, we generated mixed BM chimeras in which lethally irradiated WT recipients were reconstituted with a 1:1 mixture of WT:*Tnfr1*⁻/⁻ BM or entirely with *Tnfr1*⁻/⁻ BM as a positive control. Importantly, there was no competitive defect in the reconstitution of *Tnfr1*⁻/⁻ cells in the mixed chimera setting, nor a competitive defect in the recruitment of *Tnfr1*⁻/⁻ cells to intestinal PG, as these mice contained a 1:1 ratio of WT and *Tnfr1*⁻/⁻ immune cells within both the spleen and PG (Fig. S4 C). Strikingly, IL-1 production was reduced in both monocytes and neutrophils lacking TNFR1 relative to WT cells within the same mice, demonstrating that cell-intrinsic TNFR1 signaling mediates optimal production of IL-1 in monocytes and neutrophils (Fig. 4, C and D; and Fig. S4 D). Moreover, TNF levels were reduced in both monocytes and neutrophils lacking TNFR1 relative to WT cells isolated from the same intestinal PG, demonstrating that TNFR1 signals in a feedforward loop to promote TNF production in a cell-intrinsic fashion (Fig. S4 E). Notably, Toll-like receptor 4 (TLR4) was not required for enhanced expression of TNF or IL-1 by monocytes in response to
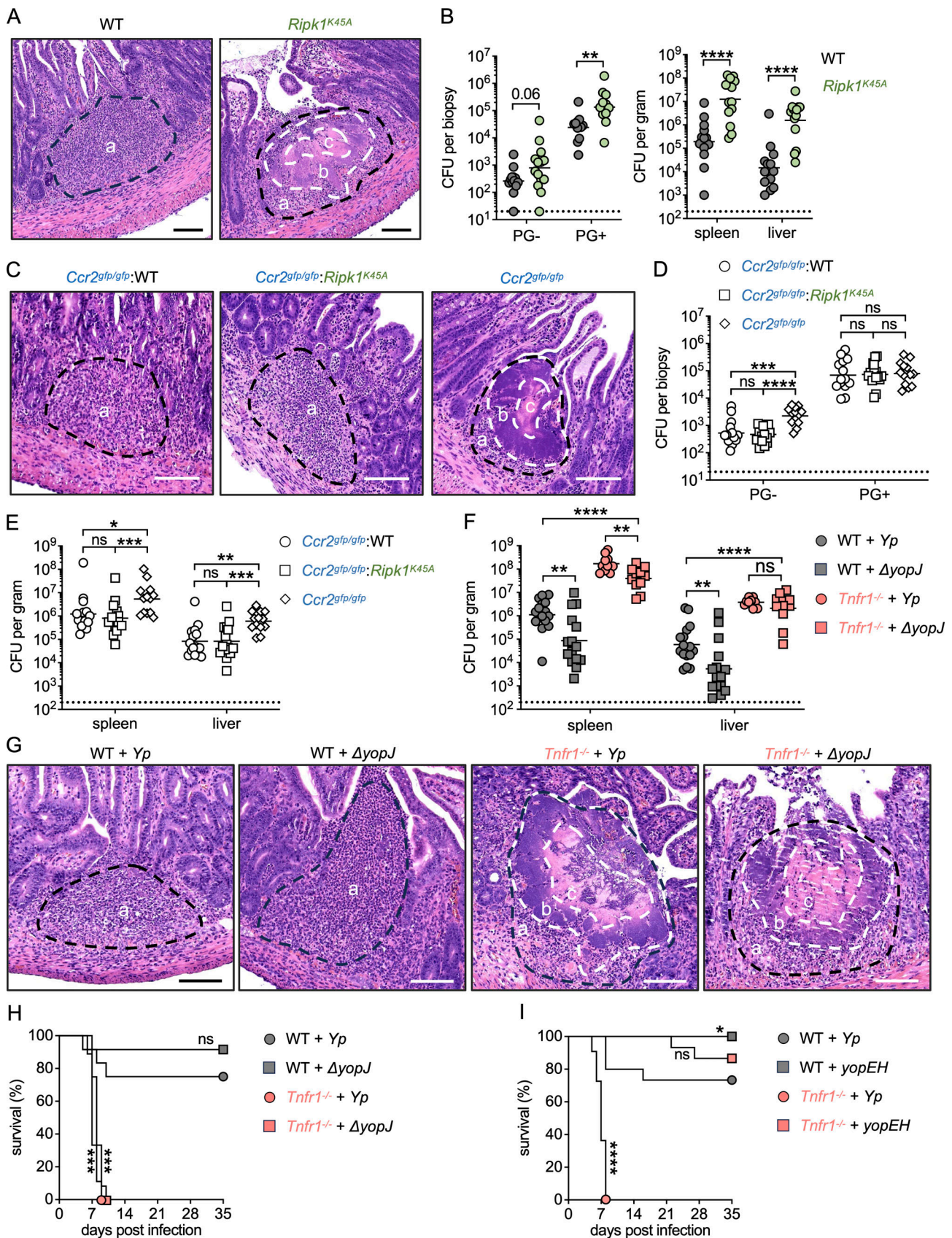
Figure 3. **TNFR1 signaling in monocytes controls *Yp* independently of RIPK1 kinase–induced cell death. (A)** H&E-stained paraffin-embedded small intestinal sections from *WT* (left) and *Ripk1^{K45A}* (right) mice at day 5 after *Yp* infection; a (black dashed lines) = immune cell infiltrate, b = bacterial colony, c = necrosis. White dashed lines delineate the edges of central necrosis and extracellular bacterial colonies. Scale bars = 100 μm. Images representative of two

independent experiments. **(B)** Bacterial burdens in small intestinal PG$^-$ and PG$^+$ tissue (left) and indicated organs (right) of WT and *Ripk1*^{K45A} mice at day 5 after *Yp* infection. Each circle represents one mouse. Lines represent the geometric mean. Pooled data from two independent experiments. **(C)** H&E-stained paraffin-embedded small intestinal sections from chimeric WT mice reconstituted with either *Ccr2*$^{gfp/gfp}$:WT (left), *Ccr2*$^{gfp/gfp}$:*Ripk1*^{K45A} (middle), or *Ccr2*$^{gfp/gfp}$ (right) BM at day 5 after *Yp* infection. a (black dashed lines) = immune cell infiltrate, b = bacterial colony, c = necrosis. White dashed lines delineate the edges of central necrosis and extracellular bacterial colonies. Scale bars = 100 μm. Representative images of two independent experiments. **(D)** Bacterial burdens in small intestinal PG$^-$ and PG$^+$ tissue of chimeric WT mice reconstituted with either *Ccr2*$^{gfp/gfp}$:WT (circles), *Ccr2*$^{gfp/gfp}$:*Ripk1*^{K45A} (squares), or *Ccr2*$^{gfp/gfp}$ (diamonds) at day 5 after *Yp* infection. Each symbol represents one mouse. Lines represent the geometric mean. Pooled data from two independent experiments. **(E)** Bacterial burdens in indicated organs of chimeric WT mice reconstituted with either *Ccr2*$^{gfp/gfp}$:WT (circles), *Ccr2*$^{gfp/gfp}$:*Ripk1*^{K45A} (squares), or *Ccr2*$^{gfp/gfp}$ (diamonds) at day 5 after *Yp* infection. Each symbol represents one mouse. Lines represent the geometric mean. Pooled data from two independent experiments. **(F)** Bacterial burdens in indicated organs of WT (gray) and *Tnfr1*$^{-/-}$ (red) mice infected with WT (circles) or *ΔyopJ* (squares) *Yp* at day 5 after infection. Each symbol represents one mouse. Lines represent the geometric mean. Pooled data from four independent experiments. **(G)** H&E-stained paraffin-embedded small intestinal sections from WT and *Tnfr1*$^{-/-}$ mice infected with either WT or *ΔyopJ Yp* at day 5 after infection. a (black dashed lines) = immune cell infiltrate, b = bacterial colony, c = necrosis. White dashed lines delineate the edges of central necrosis and extracellular bacterial colonies. Scale bars = 100 μm. Representative images of three independent experiments. **(H)** Survival of WT (gray) and *Tnfr1*$^{-/-}$ (red) mice infected with WT (circles) or *ΔyopJ* (squares) *Yp*. n = 9–12 mice per group. Pooled data from two independent experiments. **(I)** Survival of WT (gray) or *Tnfr1*$^{-/-}$ (red) mice infected with WT (circles) or *yopEH* (squares) *Yp*. n = 11–15 mice per group. Pooled data from two independent experiments. Statistical analysis by Mann–Whitney U test (B), Kruskal–Wallis test with Dunn's multiple comparisons correction (D–F), and Mantel–Cox test (H and I). $^*P < 0.05$, $^{**}P < 0.01$, $^{***}P < 0.001$, $^{****}P < 0.0001$, ns = not significant.

Yp infection or control of bacterial burdens in PG$^-$ or PG$^+$ intestinal tissues, indicating that other TLRs or pattern recognition receptors detect *Yp* to promote inflammatory cytokine production and bacterial restriction (Fig. S4, F and G). Overall, these data show that cell-intrinsic TNFR1 signaling promotes optimal IL-1 production in myeloid cells within intestinal PG, raising the question of whether IL-1 production downstream of TNFR1 signaling in monocytes contributes to control of *Yp* during early intestinal infection.

IL-1 signaling is required for PG formation and intestinal control of *Yp*

IL-1 plays a critical role in host defense against other pathogens by promoting immune cell recruitment and activation, cytokine production, angiogenesis, and vascular permeability (Franchi et al., 2012; Barry et al., 2013; Copenhaver et al., 2015; Lee et al., 2015; Fahey and Doyle, 2019; Liu et al., 2020). Mice lacking IL-1 signaling are more susceptible to systemic *Yp* infection (Vladimer et al., 2012; Ratner et al., 2016; Chen et al., 2021). However, IL-1β can also promote increased intestinal permeability and barrier dysfunction during *Yp* infection (Meinzer et al., 2012), suggesting multifaceted roles for IL-1 signaling within specific compartments and stages of infection. To test the contribution of IL-1 signaling in the control of enteric *Yp* infection within PGs, we performed oral *Yp* infections in *Il1r1*$^{-/-}$ mice, which lack IL-1R and thus cannot respond to IL-1 cytokines. Notably, the intestinal lesions in *Il1r1*$^{-/-}$ mice contained a central area of tissue necrosis surrounded by expanded bacterial microcolonies (Fig. 5, A and B), remarkably similar to the necrosuppurative intestinal lesions seen in *Ccr2*$^{gfp/gfp}$ mice (Sorobetea et al., 2023) and *Tnfr1*$^{-/-}$ mice (Fig. 1 A and Fig. 5 A). Further, at day 5 after infection, *Il1r1*$^{-/-}$ mice had significantly higher intestinal bacterial burdens than WT mice, specifically in PG$^+$ and PG$^-$ tissue and Peyer's patches (Fig. 5 C and Fig. S5 A). Myeloid cells in IL-1R–deficient mice also failed to contain *Yp* microcolonies as determined by immunofluorescence microscopy (Fig. 5 D). This failure to contain bacteria within organized PGs was reflected in decreased survival of *Il1r1*$^{-/-}$ mice relative to WT mice (Fig. 5 E). However, at day 5 after infection, bacterial burdens in systemic organs were only moderately increased

compared with those of WT mice (Fig. S5 B), suggesting that IL-1–independent mechanisms of systemic bacterial control operate downstream of TNF signaling during acute infection.

Given that mice defective in TNFR1 signaling had impaired neutrophil activation and reduced myeloid cell numbers within PGs, we considered the possibility that IL-1R signaling also plays a role in neutrophil recruitment and activation during *Yp* infection. Intriguingly, while *Il1r1*$^{-/-}$ PG contained similar numbers of monocytes and macrophages as WT PG, they had significantly fewer neutrophils (Fig. 5 F). Surface expression of the neutrophil activation marker CD11b was also significantly reduced in *Il1r1*$^{-/-}$ PG compared with WT PG (Fig. 5 G). Furthermore, levels of the neutrophil-recruiting chemokine CXCL1 were also significantly reduced in *Il1r1*$^{-/-}$ PG compared with WT PG (Fig. 5 H). Interestingly, CCL2, CCL4, and IL-6 levels were similar between *Il1r1*$^{-/-}$ and WT PG, indicating that this effect was specific to CXCL1 (Fig. S5 C). IL-1R is activated by both IL-1α and IL-1β, which have unique and shared functions (Dinarello, 2018). Notably, compared with WT mice, both *Il1a*$^{-/-}$ and *Il1b*$^{-/-}$ mice had elevated bacterial burdens in PG$^+$ tissue and PP but not in PG$^-$ tissue (Fig. 5 I and Fig. S5 A), in contrast to *Il1r1*$^{-/-}$ mice, which had elevated bacterial burdens in all three intestinal compartments. Moreover, similar to *Il1r1*$^{-/-}$ mice, mice lacking either IL-1α or IL-1β had relatively mild increases in bacterial burdens in systemic organs as compared with WT mice on day 5 after infection (Fig. S5, D and E). Intriguingly, *Il1a*$^{-/-}$ mice had a survival defect comparable with that of *Il1r1*$^{-/-}$ mice, whereas *Il1b*$^{-/-}$ mice had similar survival to WT mice following *Yp* infection (Fig. 5 J). These data suggest that while IL-1α and IL-1β contribute nonredundantly to early control of enteric *Yp* infection in PGs, IL-1α is more important than IL-1β in promoting host survival. Collectively, these results indicate that IL-1R signaling is important for the control of enteric *Yp* infection in intestinal PGs and contributes to intestinal neutrophil recruitment and activation.

Monocyte-derived IL-1 signals to non-hematopoietic cells to restrict *Yp* in intestinal PGs

Our findings demonstrate that autocrine TNF signaling in inflammatory monocytes promotes cell-intrinsic IL-1 production
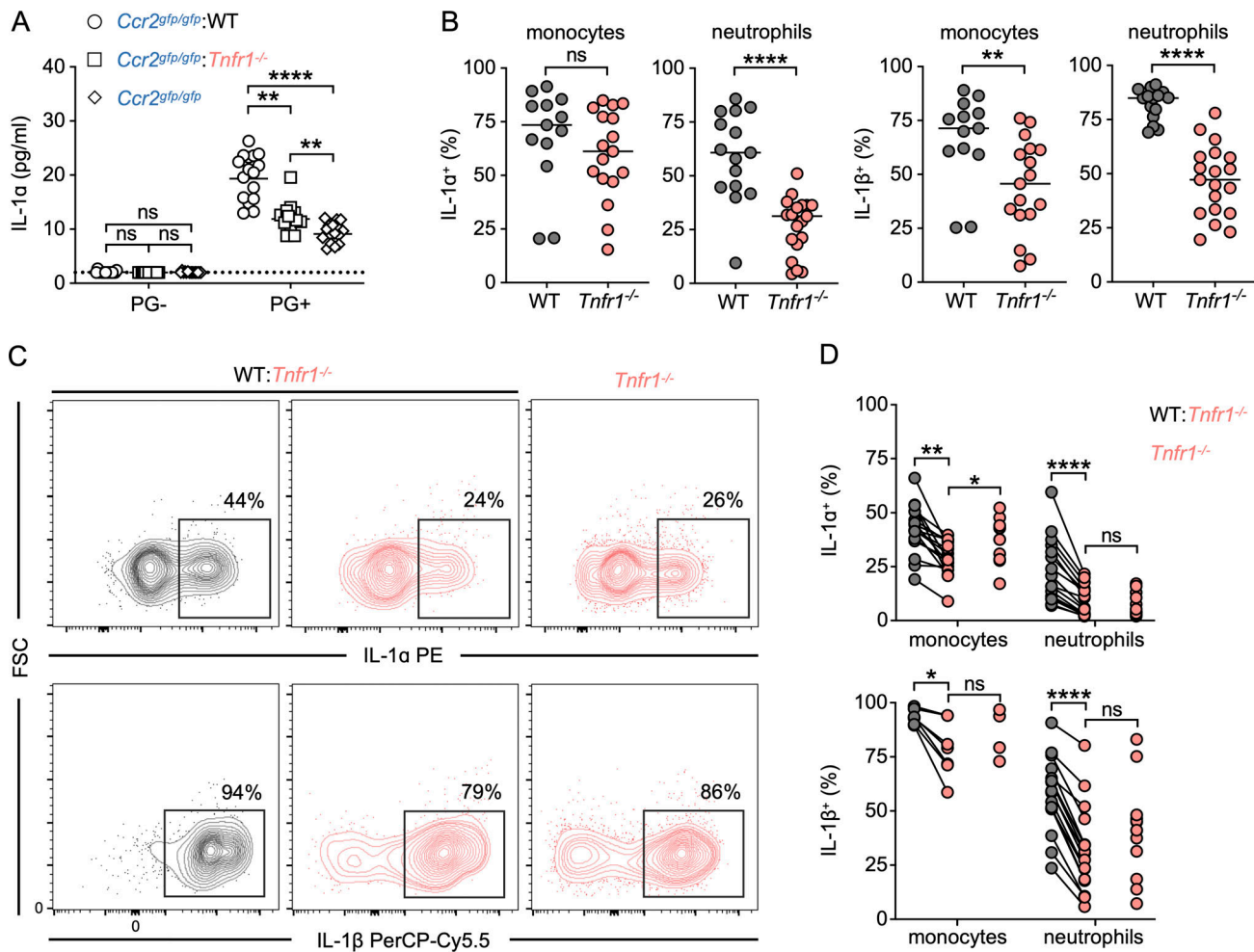
Figure 4. **Cell-intrinsic TNFR1 signaling is required for maximal IL-1 production within intestinal PGs during *Yp* infection. (A)** Cytokine levels in tissue punch biopsy homogenates isolated 5 days after infection of chimeric WT mice reconstituted with indicated donor cells. Each symbol represents the mean of 3–10 pooled punch biopsies from one mouse. Lines represent the median. Pooled data from two independent experiments. **(B)** Frequency of IL-1α– or IL-1β–producing monocytes and neutrophils isolated from small intestinal PG+ tissue 5 days after infection. Each circle represents the mean of 3–10 pooled punch biopsies from one mouse. Lines represent the median. Pooled data from three independent experiments. **(C)** Flow cytometry plots of intracellular IL-1 staining in monocytes (CD64+ Ly-6C^hi) from small intestinal PG+ tissue at day 5 after infection. Plots representative of two independent experiments. **(D)** Intracellular IL-1 staining in monocytes and neutrophils in small intestinal PG+ tissue at day 5 after infection. Each circle represents the mean of 3–10 pooled punch biopsies from one mouse. Lines connect congenic cell populations within individual mice. Pooled data from two independent experiments. Statistical analysis by Kruskal–Wallis test with Dunn's multiple comparisons correction (A), Mann–Whitney U test (B), and for congenically marked cells within mice: Wilcoxon test; across groups: Mann–Whitney U test (D). *P < 0.05, **P < 0.01, ****P < 0.0001, ns = not significant.

and subsequent IL-1R signaling promotes anti-*Yp* immune defense. However, whether monocyte-derived IL-1 is specifically required for the control of intestinal *Yp* has not been tested. We therefore infected mixed BM chimeras in which irradiated WT recipient mice were reconstituted with a 1:1 ratio of *Il1ab*^−/−:*Ccr2*^gfp/gfp BM cells to generate cohorts of mice lacking IL-1α and IL-1β production in monocytes (Fig. S5 F). Critically, these mice had significantly elevated bacterial burdens in PG, Peyer's patches, spleen, and liver compared with control mice (Fig. 6, A and B; and Fig. S5 G). Bacterial burdens in PG− biopsies were elevated in mice entirely lacking hematopoietic IL-1 but not in mice with monocyte-specific IL-1 deficiency. Together, these results suggest that IL-1 production from monocytes is important for bacterial restriction in intestinal compartments and systemic organs, although IL-1 production from non-monocytic

cell types also contributes to restriction of intestinal infection within PG.

IL-1R signaling within the non-hematopoietic compartment is critical for antibacterial defense against other bacterial pathogens (Homaidan et al., 2001; Moon et al., 2014; Lee et al., 2015; Bohrer et al., 2018; Liu et al., 2020; Barnett et al., 2022). To test whether IL-1R in the non-hematopoietic compartment might be important for the formation of intestinal PG and restriction of *Yp*, we reconstituted lethally irradiated *Il1r1*^−/− mice with WT BM (Fig. S5 H). Notably, mice lacking IL-1R in non-hematopoietic cells had elevated bacterial burdens in both intestinal (PP, PG) and systemic (liver and spleen) tissues following oral *Yp* infection compared with WT control chimeras, while mice lacking IL-1R in the hematopoietic compartment had bacterial burdens similar to those observed in the WT control
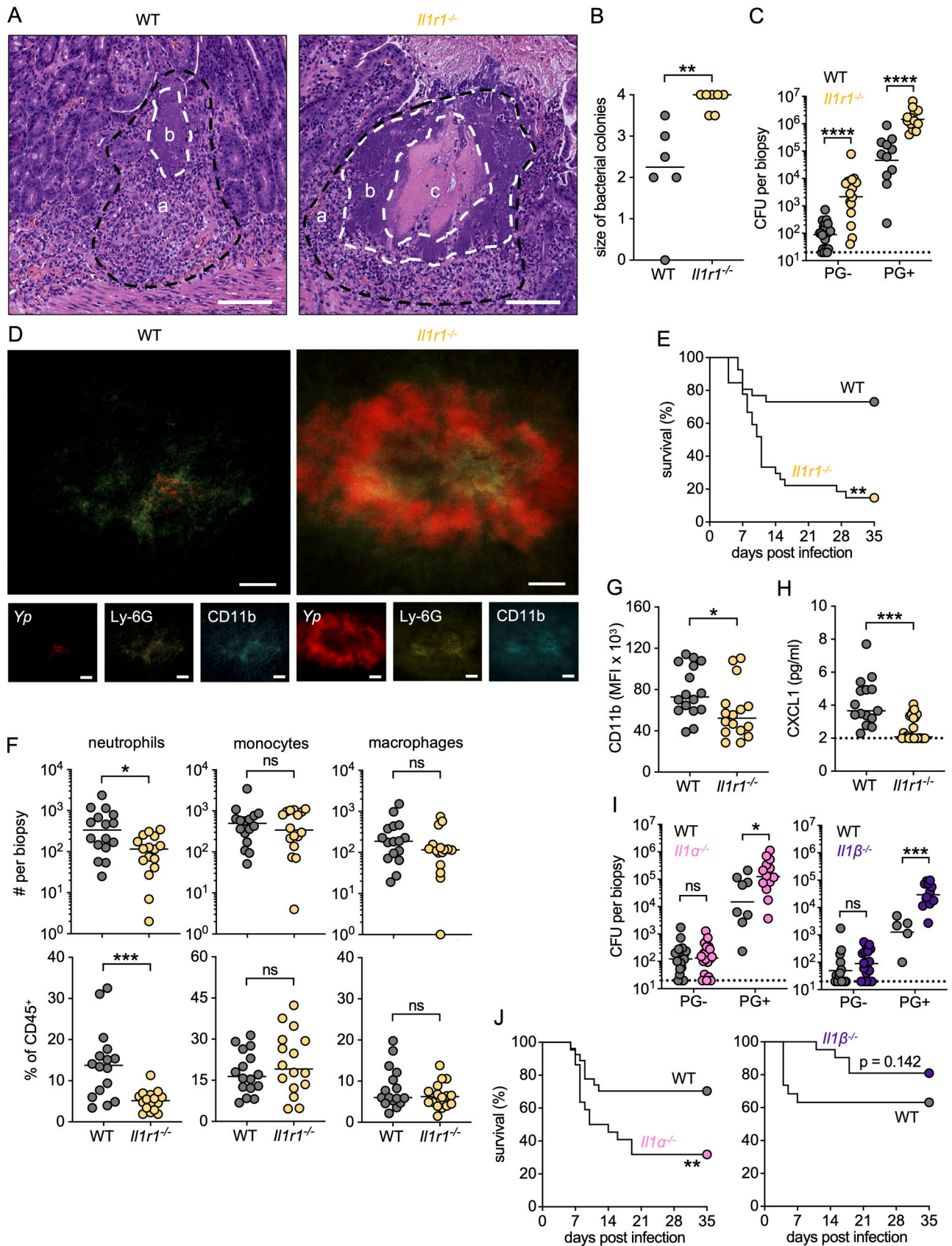
Figure 5. **IL-1 signaling is required for PG formation and intestinal control of *Yp*. (A)** H&E-stained paraffin-embedded small intestinal sections from *Yp*-infected mice at day 5 after infection; a (black dashed lines) = immune cell infiltrate, b = bacterial colony, c = necrosis. White dashed lines delineate the edges of central necrosis and extracellular bacterial colonies. Representative images of one experiment. Scale bars = 250 μm. **(B)** Histopathological scores of small

intestinal tissue from uninfected or *Yp*-infected mice at day 5 after infection. Each mouse was scored between 0 and 4 (minimal to extensive) for the size of the bacterial colony. Each circle represents one mouse. Lines represent the median. Pooled data from two experiments. **(C)** Bacterial burdens in small intestinal PG⁻ and PG⁺ tissues isolated 5 days after infection. Each circle represents the mean of three to five pooled punch biopsies from one mouse. Lines represent the geometric mean. Pooled data from three independent experiments. **(D)** Fluorescently labeled whole-mount small intestinal PG⁺ tissue from *Yp*-infected WT (left) and *Il1r1⁻/⁻* (right) mice at day 5 after infection. Red (*Yp*-mCherry), yellow (Ly-6G-AF647), blue (CD11b-AF700). Scale bars = 100 μm. Representative image of two independent experiments. **(E)** Survival of infected WT (n = 26) and *Il1r1⁻/⁻* (n = 20) mice. Pooled data from two independent experiments. **(F)** Total numbers (top) and frequencies (bottom) of neutrophils, monocytes, and macrophages in PG⁺ small intestinal tissue isolated 5 d after infection. Each circle represents the mean of 3–20 pooled punch biopsies from one mouse. Lines represent the median. Pooled data from three independent experiments. **(G)** CD11b surface expression on neutrophils in PG⁺ tissue at day 5 after infection. Each circle represents the mean of 3–10 pooled punch biopsies from one mouse. Lines represent the median. Data representative of three independent experiments. **(H)** CXCL1 levels in PG⁺ tissue punch biopsy homogenates isolated 5 days after infection. Each datapoint represents the mean of 3–20 pooled punch biopsies from one mouse. Lines represent the median. Pooled data from three independent experiments. **(I)** Bacterial burdens in small intestinal PG⁻ and PG⁺ tissues at day 5 after infection of indicated genotypes. Each circle represents the mean of three to five pooled punch biopsies from one mouse. Lines represent the geometric mean. Pooled data from three independent experiments. **(J)** Survival of infected WT (left: n = 27; right: n = 19), *Il1a⁻/⁻* (n = 22), and *Il1b⁻/⁻* (n = 21) mice. Pooled data from (left) three and (right) two independent experiments. Statistical analysis by Mann–Whitney U test (B, C, and F–I) and Mantel–Cox test (E and J). *P < 0.05, **P < 0.01, ***P < 0.001, ****P < 0.0001, ns = not significant.

Discussion

The enteric pathogen *Yp* induces the formation of PGs in both the human and murine intestine (El-Maraghi and Mair, 1979; Lamps et al., 2001; Kojima et al., 2007; Rohena et al., 2014; Davis et al., 2015; Richardson et al., 2018; Zhang et al., 2018; Sorobetea et al., 2023). We previously described PGs histopathologically within MLN (Peterson et al., 2017), as well as within the lamina propria of the gastrointestinal tract (Sorobetea et al., 2023), based on the presence of a central core of cell debris surrounded by dense cuffs of neutrophils and epithelioid macrophages within these structures (Peterson et al., 2017). Here, we uncover a crucial myeloid TNF/IL-1 signaling circuit that restricts *Yp* replication within intestinal PGs. Notably, in the absence of protective TNFR1 and IL-1R1 signals, mice exhibited defective control of *Yp* and had PGs with central areas of necrosis and expanded bacterial colonies not seen in WT mice.

TNF plays an important role in bacterial granuloma formation and maintenance (Kindler et al., 1989; Flynn et al., 1995; Bean et al., 1999; Roach et al., 2002; Algood et al., 2005; Chakravarty et al., 2008; Clay et al., 2008; Lin et al., 2010). Anti-TNF therapy triggers the reactivation of dormant *Mycobacterium tuberculosis* infection (Botha and Ryffel, 2003; Chakravarty et al., 2008; Matty et al., 2015). TNF also promotes macrophage-dependent control of bacterial replication within granulomas during chronic *Salmonella* infection (Pham et al., 2020). TNF promotes multiple antimicrobial activities of macrophages that are critical for granuloma formation and control of tuberculosis (Flynn et al., 1995; Bean et al., 1999; Clay et al., 2008; Tobin et al., 2010). However, excessive TNF causes macrophage cell death that can be detrimental to bacterial control (Tobin et al., 2012). Here, we find that autocrine TNF signaling on monocyte-lineage cells promotes cell-intrinsic production of IL-1, which signals through non-hematopoietic IL-1R to control *Yp* bacterial burdens within intestinal PGs. Our findings highlight a key role for TNF

signaling in the control of *Yp* infection within intestinal PGs. However, *Yp* YopJ suppresses cell-intrinsic inflammatory cytokine expression (Palmer et al., 1998), raising the question of how anti-*Yp* immune responses are initiated. During *Legionella pneumophila* infection, IL-1 signaling induces TNF production in uninfected bystander cells, thus bypassing *Legionella* virulence factor–induced blockade of host protein synthesis (Copenhaver et al., 2015; Liu et al., 2020). Bystander cells not injected with YopJ are thus a potential source of TNF or IL-1 during *Yp* infection (Peterson et al., 2017).

TNFR1 signaling promotes *Yp*-induced cell death via RIPK1 activity, and RIPK1 kinase activity is necessary for the control of *Yp* infection (Peterson et al., 2017). However, while RIPK1 kinase activity was essential for intestinal PG architecture, inflammatory monocytes did not require RIPK1 kinase activity for PG formation and *Yp* restriction. These findings suggest that two distinct pathways mediate protection against enteric *Yp* infection: a monocyte-intrinsic TNFR1 pathway that amplifies IL-1 cytokine production, and a separate pathway involving RIPK1 kinase–mediated cell death of non-monocytic cells in response to YopJ-induced blockade of immune signaling. Notably, neutrophils undergo gasdermin E–dependent pyroptosis downstream of RIPK1 kinase activity, which contributes to the restriction of *Yp* infection in vivo (Chen et al., 2021). Future studies will elucidate whether RIPK1 kinase–induced neutrophil cell death enables control of *Yp*.

TNF promotes IL-1β expression in dendritic cells (Jain et al., 2020) and tumor-associated macrophages (Caronni et al., 2023). In human macrophages, TNF promotes IL-1β expression via sterol response element binding protein (Kusnadi et al., 2019). Our findings indicate that monocyte-derived IL-1 controls *Yp* infection independent of RIPK1 kinase–mediated monocyte cell death. Monocytes may release IL-1 through inflammasome-dependent pyroptosis or in a "hyperactivated" state, whereby cells release IL-1 in a gasdermin D–dependent manner in the absence of pyroptosis (Chen et al., 2014; Gaidt et al., 2016; Evavold et al., 2018; Aizawa et al., 2020; Zhivaki et al., 2020). Future studies will clarify mechanisms of IL-1 expression and release downstream of TNF during *Yp* infection.

IL-1R signaling is critical for bacterial control during tuberculosis infection, and the loss of IL-1R signaling leads to necrotic
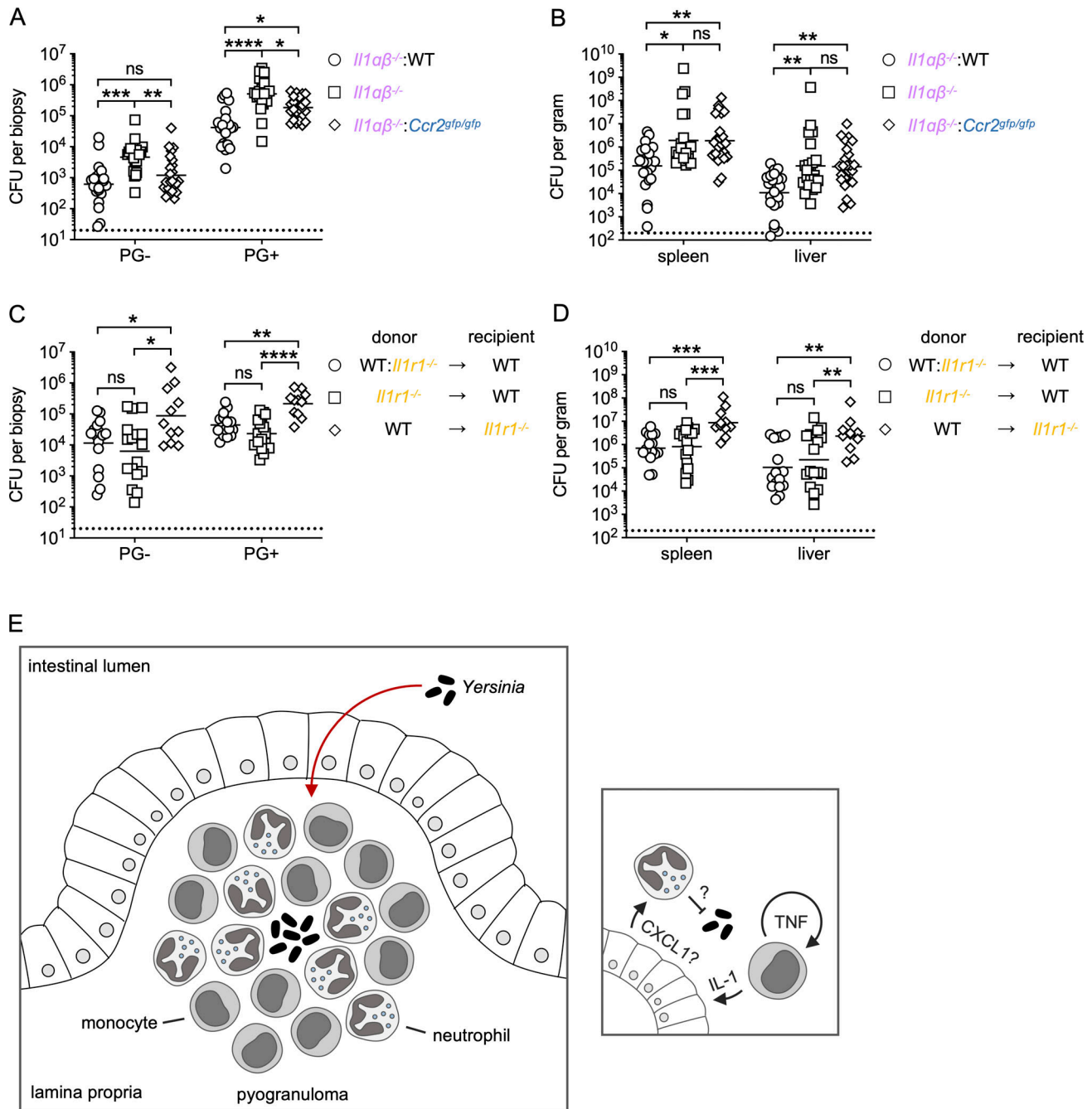
Figure 6. **Monocyte-derived IL-1 signals to non-hematopoietic cells to restrict *Yp* in intestinal PGs. (A)** Bacterial burdens in small intestinal PG⁻ and PG⁺ tissues at day 5 after infection of indicated chimeric mice. Each symbol represents the mean of three to five pooled punch biopsies from one mouse. Lines represent the geometric mean. Data were pooled from four independent experiments. **(B)** Bacterial burdens in the indicated organ at day 5 after infection of indicated chimeric mouse. Each symbol represents one mouse. Lines represent the geometric mean. Pooled data from four independent experiments. **(C)** Bacterial burdens in small intestinal PG⁻ and PG⁺ tissues at day 5 after infection of indicated chimeric mice. Each symbol represents the mean of three to five pooled punch biopsies from one mouse. Lines represent the geometric mean. Pooled data from three independent experiments. **(D)** Bacterial burdens in indicated organs at day 5 after infection of the indicated chimeric mouse. Each symbol represents one mouse. Lines represent the geometric mean. Data were pooled from three independent experiments. **(E)** Model of TNF-IL-1 circuit mediated by monocytes and non-hematopoietic cells to restrict *Yp* infection within intestinal PGs. All statistical analyses by Kruskal–Wallis test with Dunn's multiple comparisons correction. *P < 0.05, **P < 0.01, ***P < 0.001, ****P < 0.0001, ns = not significant.

lesions in the lung (Yamada et al., 2000; Sugawara et al., 2001; Mayer-Barber et al., 2010, 2011; Di Paolo et al., 2015; Ji et al., 2019; Silvério et al., 2021). Here, we observed that in the absence of IL-1R, intestinal PGs exhibited a necrotic pathology associated

with elevated intestinal *Yp* burdens. Unexpectedly, systemic bacterial burdens were similar between WT and *Il1r1*⁻/⁻ mice, suggesting that TNF engages IL-1–independent pathways to restrict systemic bacterial replication. Mice lacking IL-1R signaling

were more susceptible than mice lacking IL-1α or IL-1β alone, indicating that both IL-1 cytokines contribute non-redundantly to bacterial control. While mice deficient in IL-1α exhibited elevated mortality, IL-1β–deficient mice did not. During the early intestinal stage of infection, IL-1α and IL-1β may mediate overlapping mechanisms of Yp restriction, while at later stages, IL-1α plays a unique role in Yp control. IL-1α mediates intestinal inflammation and inflammatory cell recruitment during $Yersinia$ $enterocolitica$ infection (Dube et al., 2001). In contrast, IL-1β contributes to Yp restriction (Chen et al., 2021), but also promotes intestinal barrier permeability and translocation of intestinal bacteria downstream of YopJ activity (Jung et al., 2012). Tight regulation of intestinal IL-1 signaling may therefore be important to combat Yp infection while avoiding excessive tissue damage.

While IL-1β is released from hematopoietic cells downstream of inflammasome activation, IL-1α is more broadly expressed across cell types and can function within the nucleus as a cell surface–associated cytokine or as an alarmin released from dying cells (Dinarello, 2018). Monocyte-specific loss of both IL-1α and IL-1β led to defective control of Yp within intestinal PG. However, IL-1α and IL-1β production from monocytes was dispensable for control of Yp burdens in PG− tissue and systemic organs, suggesting that other cell types contribute to IL-1–mediated bacterial restriction in these compartments. TNFR1 signaling also promoted neutrophil IL-1 production during enteric Yp infection, in line with prior studies identifying a role for GSDME-dependent IL-1β production by neutrophils in the control of enteric Yp infection (Chen et al., 2021). Additionally, epithelial cells are a major source of IL-1α that drives inflammation during intestinal injury (Bersudsky et al., 2014; Scarpa et al., 2015). Whether neutrophils, epithelial cells, or other cell types produce IL-1 to control intestinal Yp remains to be investigated. Interestingly, several other IL-1 family members, including IL-18 and IL-33, have been linked to granuloma formation in the setting of sarcoidosis or schistosomiasis, and IL-18 also contributes to host defense against $Yersinia$ $pestis$ (Greene et al., 2000; Townsend et al., 2000; Vladimer et al., 2012; Ratner et al., 2016). Future studies will investigate the potential role of other IL-1 family cytokines within PGs during intestinal Yp infection.

Our observations that IL-1R on stromal cells is critical for the control of Yp infection highlights a recurring theme of IL-1–mediated crosstalk between immune and non-immune cells during infection (Lee et al., 2015; Bohrer et al., 2018; Orzalli et al., 2018; Liu et al., 2020; Overcast et al., 2023). IL-1R is expressed in non-lymphoid tissues, including epithelial and endothelial cells (Deyerle et al., 1992), suggesting a general mechanism by which non-hematopoietic cells amplify and coordinate antipathogen defense. The cellular subpopulations within the intestine that respond to IL-1 and their downstream effector functions that restrict Yp remain unknown. IL-1R signaling upregulates antimicrobial peptide expression, promotes neutrophil recruitment, and modulates intestinal permeability (Homaidan et al., 2001; Yan et al., 2006; Al-Sadi and Ma, 2007; Franchi et al., 2012; Moon et al., 2014; Lee et al., 2015; Overcast et al., 2023). We observed decreased neutrophil recruitment in mice lacking monocytes (Sorobetea et al., 2023), TNFR1, or IL-1R,

and IL-1R deficiency was associated with decreased CXCL1 levels within PGs. Altogether, our work uncovers a monocyte-intrinsic TNF/IL-1 circuit that signals to IL-1R on stromal cells to control Yp infection, providing new insight into the cytokine networks within enteric PG that mediate the control of bacterial pathogens.

Materials and methods

Mice
C57BL/6J (CD45.2), C57BL/6.SJL (CD45.1), $Tnfr2^{-/-}$ (Erickson et al., 1994), and $Ccr2^{gfp/gfp}$ mice (Satpathy et al., 2013) were obtained from the Jackson Laboratory. $Tnfr1^{-/-}$ (Pfeffer et al., 1993), $Ripk1^{K45A}$ (Berger et al., 2014), $Il1r1^{-/-}$ (Glaccum et al., 1997), $Tlr4^{-/-}$ (Hoshino et al., 1999), $Il1a^{-/-}$ (Horai et al., 1998), $Il1b^{-/-}$ (Horai et al., 1998), and $Il1a^{-/-}Il1b^{-/-}$ (Horai et al., 1998) mice were previously described. All mice were bred at the University of Pennsylvania by homozygous mating and housed separately by genotype. Mice of either sex between 8 and 12 wk of age were used for all experiments. All animal studies were performed in strict accordance with University of Pennsylvania Institutional Animal Care and Use Committee–approved protocols (protocol #804523).

Bacteria
WT Yp (clinical isolate strain 32777, serogroup O1) (Simonet and Falkow, 1992) and isogenic YopJ-deficient mutant were provided by Dr. James Bliska (Dartmouth College, Hanover, NH, USA) and previously described (Philip et al., 2014). Mutants lacking YopE ($\Delta yopE$), YopH enzymatic activity (YopH^{R409A}), or both (denoted $yopEH$) were previously described (Sorobetea et al., 2023).

BM chimeras
WT B6.SJL mice (CD45.1 background) or knockout mice ($Tnfr1^{-/-}$ or $Il1r1^{-/-}$, CD45.2 background) were lethally irradiated (1,096 rads). B6.SJL mice were obtained from the Jackson Laboratory and therefore microbiota-matched. 6 h later, mice were injected retro-orbitally with freshly isolated BM cells (5 × 10^6 total cells, 2.5 × 10^6 cells per donor in mixed groups) from isogenic donors of the indicated genotypes. All chimeras were provided with antibiotic-containing acidified water (40 mg trimethoprim and 200 mg sulfamethoxazole per 500 ml drinking water) for 4 wk after irradiation and subsequently provided acidified water without antibiotics for a total of at least 10 wk. The reconstitution of hematopoietic cells (proportion of donor CD45$^+$ cells among total CD45$^+$ cells) in the blood, spleen, or intestine was analyzed by flow cytometry.

Mouse infections
Yp was cultured to stationary phase at 28°C and 250 rpm shaking for 16 h in 2xYT broth supplemented with 2 µg/ml triclosan (Millipore Sigma). Mice were fasted for 16 h and subsequently inoculated by oral gavage with 200 µl phosphate-buffered saline (PBS) as previously described (Sorobetea et al., 2023) All bacterial strains were administered at 2 × 10^8 CFU per mouse.

Bacterial CFU quantifications
Tissues were collected in sterile PBS, weighed, and homogenized for 40 s with 6.35-mm ceramic spheres (MP Biomedical) using a

FastPrep-24 bead beater (MP Biomedical). Samples were serially diluted 10-fold in PBS, plated on LB agar supplemented with 2 µg/ml triclosan, and incubated for 2 days at room temperature. Dilutions of each sample were plated in triplicate and expressed as the mean CFU per gram or per biopsy.

Cytokine quantification

Cytokines were measured in homogenized tissue supernatants using a Cytometric Bead Array (BD Biosciences) according to the manufacturer's instructions with the following modification: the amounts of capture beads, detection reagents, and sample volumes were scaled down 10-fold. Data were collected on an LSRFortessa flow cytometer (BD Biosciences) and analyzed with FlowJo v10 (BD Biosciences).

Tissue preparation and cell isolation

Blood was harvested by cardiac puncture upon euthanasia and collected in 250 U/ml Heparin solution (Millipore Sigma). Erythrocytes were lysed with a red blood cell lysing buffer (Millipore Sigma).

Spleens were homogenized through a 70-µm cell strainer (Thermo Fisher Scientific), then flushed with R10 buffer consisting of RPMI 1640 (Millipore Sigma) supplemented with 10 mM HEPES (Millipore Sigma), 10% fetal bovine serum (Omega Scientific), 1 mM sodium pyruvate (Thermo Fisher Scientific), and 100 U/ml penicillin + 100 µg/ml streptomycin (Thermo Fisher Scientific). Erythrocytes were lysed with a red blood cell lysing buffer (Millipore Sigma).

Intestines were excised, flushed luminally with sterile PBS to remove the feces, opened longitudinally along the mesenteric side, and placed luminal side down on cutting boards (Epicurean). Small intestinal tissue containing macroscopically visible PGs (PG+), adjacent non-granulomatous areas (PG−), and uninfected control tissue were excised using a 2-mm-diameter dermal punch-biopsy tool (Keyes). Biopsies within each mouse were pooled groupwise, suspended in epithelial dissociation buffer consisting of calcium and magnesium-free HBSS (Thermo Fisher Scientific) supplemented with 15 mM HEPES, 10 mg/ml bovine serum albumin (Millipore Sigma), 5 mM EDTA (Millipore Sigma), and 100 U/ml penicillin + 100 µg/ml streptomycin, and then incubated for 30 mins at 37°C under continuous agitation at 300 RPM. To isolate immune cells from the lamina propria, the tissue was enzymatically digested in R10 buffer, along with 0.5 Wünsch units/ml liberase TM (Roche), 30 µg/ml DNase I (Roche), and 5 mM $CaCl_2$ for 20 min at 37°C under continuous agitation. The resulting cell suspensions were filtered through 100-µm cell strainers (Thermo Fisher Scientific) and subjected to density gradient centrifugation using Percoll (GE Healthcare). Briefly, cells were suspended in 40% Percoll and centrifuged over a 70% Percoll layer for 20 min at 600 × g with the lowest brake at room temperature. Cells collected between the layers were washed with R10 buffer for downstream analysis.

Flow cytometry

Non-specific Fc binding was blocked for 10 mins on ice with unconjugated anti-CD16/CD32 (93; Thermo Fisher Scientific).

Cells were subsequently labeled for 30 mins on ice with the following antibodies and reagents: PE-conjugated rat anti-mouse Siglec-F (E50-2440; BD Biosciences), PE-TxR or PE-Cy5–conjugated rat anti-mouse CD11b (M1/70.15; Thermo Fisher Scientific), PE-Cy5.5 or PE-Cy7-conjugated rat anti-mouse CD4 (RM4-5; Thermo Fisher Scientific), BV510-conjugated rat anti-mouse CD3e (145-2C11; BioLegend), AF700 or PerCP-Cy5.5-conjugated rat anti-mouse Ly-6C (HK1.4; Thermo Fisher Scientific), BV605-conjugated Armenian hamster anti-mouse TCRβ (H57-597; BD Biosciences), BV650-conjugated rat anti-mouse I-A/I-E (M5/114.15.2; BD Biosciences), BV711-conjugated rat anti-mouse CD8α (53-6.7; BD Biosciences), BV785-conjugated rat anti-mouse Ly-6G (1A8; Thermo Fisher Scientific), PE-Cy7 or AF647-conjugated mouse anti-mouse CD64 (X54-5/7.1; BD Biosciences), AF700-conjugated mouse anti-mouse CD45.2 (104; BioLegend), PE-Cy5-conjugated mouse anti-mouse CD45.1 (A20; Thermo Fisher), and PE-Cy5 or PE-CF594-conjugated rat anti-mouse CD45R/B220 (RA3-6B2; BD Biosciences) along with eF780 viability dye (BioLegend) diluted in PBS. Antibodies were used at 1:200 dilution and viability dye at 1:1,500 dilution.

For intracellular staining, cells isolated from indicated tissues were incubated ex vivo for 3 h at 37°C with 5% CO_2 in R10 buffer supplemented with 0.33 µl/ml GolgiStop (BD Biosciences) and 15 µg/ml DNase I. Surface proteins were stained as above, and cells were fixed for 20 min on ice with Cytofix/Cytoperm Fixation/Permeabilization solution (BD Biosciences). Intracellular cytokines were stained at 4°C overnight with FITC or PerCP-e710-conjugated rat anti-mouse IL-1β (NJTEN3; Thermo Fisher Scientific) and PE-conjugated Armenian hamster anti-mouse IL-1α (ALF-161; BioLegend). All antibodies were diluted 1:200 in Perm/Wash Buffer (BD Biosciences). Cells were acquired on an LSRFortessa flow cytometer, and data were analyzed with FlowJo v10. Cells were gated on live singlets prior to downstream analyses.

Histology

Tissues were fixed in 10% neutral-buffered formalin (Thermo Fisher Scientific) and stored at 4°C until further processed. Tissue pieces were embedded in paraffin, sectioned by standard histological techniques, and stained with hematoxylin and eosin (H&E). Slides were scanned on an Aperio VERSA using brightfield at 20× magnification. Histopathological disease scoring was performed by blinded board-certified pathologists. Tissue sections were given a score from 0 to 4 (healthy to severe) for multiple parameters, including degree of inflammatory cell infiltration, necrosis, and free bacterial colonies, along with tissue-specific parameters such as villus blunting and crypt hyperplasia.

Immunofluorescence microscopy

Small intestinal tissue was dissected and flushed with PBS. Intestines were opened longitudinally and ∼0.5 cm tissue pieces containing macroscopically visible lesions were excised. Tissues were fixed in 1% paraformaldehyde overnight, then blocked overnight at 4°C in a blocking solution containing 10% bovine serum albumin, 1 µg/ml anti-CD16/32, and 1% normal rat serum in PBS. AF647-conjugated anti-Ly-6G antibody (1A8; BioLegend) and AF700-conjugated anti-CD11b antibody (M1/80; BioLegend)

were added at 0.01 mg/ml in 100 µl PBS per sample and then whole tissue was stained for 24 h at 4°C. Samples were washed three times with PBS, mounted whole onto slides in Prolong Glass Antifade Mountant (Thermo Fisher Scientific), and cured for 2 days at room temperature. Images were acquired on a DMI 6000 laser-scanning confocal microscope (Leica) with a 10× objective. The center of the sample was determined in the Z direction and then imaged. Images were analyzed using ImageJ v2.1. Adjustments for brightness and contrast were applied to the entire image. No threshold manipulation was performed.

Statistics
Statistical analyses were performed using Prism v9.0 (GraphPad Software). Independent groups were compared by Mann–Whitney U test or Kruskal–Wallis test with Dunn's multiple comparisons test. Survival curves were compared by Mantel–Cox test. Statistical significance is denoted as * (P < 0.05), ** (P < 0.01), *** (P < 0.001), **** (P < 0.0001), or ns (not significant).

Online supplemental material
Fig. S1 further characterizes *Yp*-infected *Tnfr1*−/− and *Tnfr2*−/− mice. Fig. S2 details the chimerism of BM chimeras associated with Fig. 2. Fig. S3 details the chimerism of BM chimeras associated with Fig. 3, as well as depicting survival data of mutant *Yp* infections. Fig. S4 depicts cytokine analyses in mixed BM chimeras associated with Fig. 4, as well as cytokine data of *Tlr4*−/− mice. Fig. S5 details additional data from IL-1 chimeras associated with Figs. 5 and 6.

Data availability
Data supporting the findings of this research article are available upon request to the corresponding author.

References
Adams, K.N., K. Takaki, L.E. Connolly, H. Wiedenhoft, K. Winglee, O. Humbert, P.H. Edelstein, C.L. Cosma, and L. Ramakrishnan. 2011. Drug tolerance in replicating mycobacteria mediated by a macrophage-induced efflux mechanism. *Cell*. 145:39–53. https://doi.org/10.1016/j.cell.2011.02.022

Aizawa, E., T. Karasawa, S. Watanabe, T. Komada, H. Kimura, R. Kamata, H. Ito, E. Hishida, N. Yamada, T. Kasahara, et al. 2020. GSDME-dependent incomplete pyroptosis permits selective IL-1α release under caspase-1 inhibition. *iScience*. 23:101070. https://doi.org/10.1016/j.isci.2020.101070

Al-Sadi, R.M., and T.Y. Ma. 2007. IL-1β causes an increase in intestinal epithelial tight junction permeability. *J. Immunol.* 178:4641–4649. https://doi.org/10.4049/jimmunol.178.7.4641

Algood, H.M.S., P.L. Lin, and J.L. Flynn. 2005. Tumor necrosis factor and chemokine interactions in the formation and maintenance of granulomas in tuberculosis. *Clin. Infect. Dis.* 41:S189–S193. https://doi.org/10.1086/429994

Ali, T., S. Kaitha, S. Mahmood, A. Ftesi, J. Stone, and M.S. Bronze. 2013. Clinical use of anti-TNF therapy and increased risk of infections. *Drug Healthc. Patient Saf.* 5:79–99. https://doi.org/10.2147/DHPS.S28801

Atkinson, S., and P. Williams. 2016. Yersinia virulence factors - A sophisticated arsenal for combating host defences. *F1000Res.* 5:F1000 Faculty Rev-1370. https://doi.org/10.12688/f1000research.8466.1

Autenrieth, I.B., and J. Heesemann. 1992. In vivo neutralization of tumor necrosis factor-alpha and interferon-gamma abrogates resistance to Yersinia enterocolitica infection in mice. *Med. Microbiol. Immunol.* 181:333–338. https://doi.org/10.1007/BF00191545

Barnett, K.C., Y. Xie, T. Asakura, D. Song, K. Liang, S.A. Taft-Benz, H. Guo, S. Yang, K. Okuda, R.C. Gilmore, et al. 2022. An epithelial-immune circuit amplifies inflammasome and IL-6 responses to SARS-CoV-2. *Cell Host Microbe*. 31:243–259.e6. https://doi.org/10.1016/j.chom.2022.12.005

Barry, K.C., M.F. Fontana, J.L. Portman, A.S. Dugan, and R.E. Vance. 2013. IL-1α signaling initiates the inflammatory response to virulent Legionella pneumophila in vivo. *J. Immunol.* 190:6329–6339. https://doi.org/10.4049/jimmunol.1300100

Bean, A.G., D.R. Roach, H. Briscoe, M.P. France, H. Korner, J.D. Sedgwick, and W.J. Britton. 1999. Structural deficiencies in granuloma formation in TNF gene-targeted mice underlie the heightened susceptibility to aerosol Mycobacterium tuberculosis infection, which is not compensated for by lymphotoxin. *J. Immunol.* 162:3504–3511. https://doi.org/10.4049/jimmunol.162.6.3504

Berger, S.B., V. Kasparcova, S. Hoffman, B. Swift, L. Dare, M. Schaeffer, C. Capriotti, M. Cook, J. Finger, A. Hughes-Earle, et al. 2014. Cutting edge:

RIP1 kinase activity is dispensable for normal development but is a key regulator of inflammation in SHARPIN-deficient mice. *J. Immunol.* 192: 5476–5480. https://doi.org/10.4049/jimmunol.1400499

Bersudsky, M., L. Luski, D. Fishman, R.M. White, N. Ziv-Sokolovskaya, S. Dotan, P. Rider, I. Kaplanov, T. Aychek, C.A. Dinarello, et al. 2014. Non-redundant properties of IL-1α and IL-1β during acute colon inflammation in mice. *Gut.* 63:598–609. https://doi.org/10.1136/gutjnl-2012-303329

Black, D.S., and J.B. Bliska. 2000. The RhoGAP activity of the Yersinia pseudotuberculosis cytotoxin YopE is required for antiphagocytic function and virulence. *Mol. Microbiol.* 37:515–527. https://doi.org/10.1046/j.1365-2958.2000.02021.x

Bliska, J.B., K.L. Guan, J.E. Dixon, and S. Falkow. 1991. Tyrosine phosphate hydrolysis of host proteins by an essential Yersinia virulence determinant. *Proc. Natl. Acad. Sci. USA.* 88:1187–1191. https://doi.org/10.1073/pnas.88.4.1187

Bliska, J.B., and D.S. Black. 1995. Inhibition of the Fc receptor-mediated oxidative burst in macrophages by the Yersinia pseudotuberculosis tyrosine phosphatase. *Infect. Immun.* 63:681–685. https://doi.org/10.1128/iai.63.2.681-685.1995

Bliska, J.B., I.E. Brodsky, and J. Mecsas. 2021. Role of the Yersinia pseudotuberculosis virulence plasmid in pathogen-phagocyte interactions in mesenteric lymph nodes. *Ecosal Plus.* 9:eESP00142021. https://doi.org/10.1128/ecosalplus.ESP-0014-2021

Bohrer, A.C., C. Tocheny, M. Assmann, V.V. Ganusov, and K.D. Mayer-Barber. 2018. Cutting edge: IL-1R1 mediates host resistance to *Mycobacterium tuberculosis* by trans-protection of infected cells. *J. Immunol.* 201: 1645–1650. https://doi.org/10.4049/jimmunol.1800438

Borjesson, D.L., S.I. Simon, E. Hodzic, C.M. Ballantyne, and S.W. Barthold. 2002. Kinetics of CD11b/CD18 up-regulation during infection with the agent of human granulocytic ehrlichiosis in mice. *Lab. Invest.* 82: 303–311. https://doi.org/10.1038/labinvest.3780424

Botha, T., and B. Ryffel. 2003. Reactivation of latent tuberculosis infection in TNF-deficient mice. *J. Immunol.* 171:3110–3118. https://doi.org/10.4049/jimmunol.171.6.3110

Caronni, N., F. La Terza, F.M. Vittoria, G. Barbiera, L. Mezzanzanica, V. Cuzzola, S. Barresi, M. Pellegatta, P. Canevazzi, G. Dunsmore, et al. 2023. IL-1β⁺ macrophages fuel pathogenic inflammation in pancreatic cancer. *Nature.* 623:415–422. https://doi.org/10.1038/s41586-023-06685-2

Chakravarty, S.D., G. Zhu, M.C. Tsai, V.P. Mohan, S. Marino, D.E. Kirschner, L. Huang, J. Flynn, and J. Chan. 2008. Tumor necrosis factor blockade in chronic murine tuberculosis enhances granulomatous inflammation and disorganizes granulomas in the lungs. *Infect. Immun.* 76:916–926. https://doi.org/10.1128/IAI.01011-07

Chen, G., and D.V. Goeddel. 2002. TNF-R1 signaling: A beautiful pathway. *Science.* 296:1634–1635. https://doi.org/10.1126/science.1071924

Chen, K.W., C.J. Groß, F.V. Sotomayor, K.J. Stacey, J. Tschopp, M.J. Sweet, and K. Schroder. 2014. The neutrophil NLRC4 inflammasome selectively promotes IL-1β maturation without pyroptosis during acute Salmonella challenge. *Cell Rep.* 8:570–582. https://doi.org/10.1016/j.celrep.2014.06.028

Chen, K.W., B. Demarco, R. Ramos, R. Heilig, M. Goris, J.P. Grayczyk, C.A. Assenmacher, E. Radaelli, L.D. Joannas, J. Henao-Mejia, et al. 2021. RIPK1 activates distinct gasdermins in macrophages and neutrophils upon pathogen blockade of innate immune signaling. *Proc. Natl. Acad. Sci. USA.* 118:e2101189118. https://doi.org/10.1073/pnas.2101189118

Christofferson, D.E., Y. Li, and J. Yuan. 2014. Control of life-or-death decisions by RIP1 kinase. *Annu. Rev. Physiol.* 76:129–150. https://doi.org/10.1146/annurev-physiol-021113-170259

Clay, H., H.E. Volkman, and L. Ramakrishnan. 2008. Tumor necrosis factor signaling mediates resistance to mycobacteria by inhibiting bacterial growth and macrophage death. *Immunity.* 29:283–294. https://doi.org/10.1016/j.immuni.2008.06.011

Copenhaver, A.M., C.N. Casson, H.T. Nguyen, M.M. Duda, and S. Shin. 2015. IL-1R signaling enables bystander cells to overcome bacterial blockade of host protein synthesis. *Proc. Natl. Acad. Sci. USA.* 112:7557–7562. https://doi.org/10.1073/pnas.1501289112

Davis, J.M., and L. Ramakrishnan. 2009. The role of the granuloma in expansion and dissemination of early tuberculous infection. *Cell.* 136: 37–49. https://doi.org/10.1016/j.cell.2008.11.014

Davis, K.M., S. Mohammadi, and R.R. Isberg. 2015. Community behavior and spatial regulation within a bacterial microcolony in deep tissue sites serves to protect against host attack. *Cell Host Microbe.* 17:21–31. https://doi.org/10.1016/j.chom.2014.11.008

Delanghe, T., Y. Dondelinger, and M.J.M. Bertrand. 2020. RIPK1 kinase-dependent death: A symphony of phosphorylation events. *Trends Cell Biol.* 30:189–200. https://doi.org/10.1016/j.tcb.2019.12.009

Deyerle, K.L., J.E. Sims, S.K. Dower, and M.A. Bothwell. 1992. Pattern of IL-1 receptor gene expression suggests role in noninflammatory processes. *J. Immunol.* 149:1657–1665. https://doi.org/10.4049/jimmunol.149.5.1657

Diedrich, C.R., J. O'Hern, and R.J. Wilkinson. 2016. HIV-1 and the Mycobacterium tuberculosis granuloma: A systematic review and meta-analysis. *Tuberculosis.* 98:62–76. https://doi.org/10.1016/j.tube.2016.02.010

Dinarello, C.A. 2018. Overview of the IL-1 family in innate inflammation and acquired immunity. *Immunol. Rev.* 281:8–27. https://doi.org/10.1111/imr.12621

Dube, P.H., P.A. Revell, D.D. Chaplin, R.G. Lorenz, and V.L. Miller. 2001. A role for IL-1 alpha in inducing pathologic inflammation during bacterial infection. *Proc. Natl. Acad. Sci. USA.* 98:10880–10885. https://doi.org/10.1073/pnas.191214498

Ea, C.K., L. Deng, Z.P. Xia, G. Pineda, and Z.J. Chen. 2006. Activation of IKK by TNFalpha requires site-specific ubiquitination of RIP1 and poly-ubiquitin binding by NEMO. *Mol. Cell.* 22:245–257. https://doi.org/10.1016/j.molcel.2006.03.026

El-Maraghi, N.R.H., and N.S. Mair. 1979. The histopathology of enteric infection with Yersinia pseudotuberculosis. *Am. J. Clin. Pathol.* 71:631–639. https://doi.org/10.1093/ajcp/71.6.631

Erickson, S.L., F.J. de Sauvage, K. Kikly, K. Carver-Moore, S. Pitts-Meek, N. Gillett, K.C. Sheehan, R.D. Schreiber, D.V. Goeddel, and M.W. Moore. 1994. Decreased sensitivity to tumour-necrosis factor but normal T-cell development in TNF receptor-2-deficient mice. *Nature.* 372:560–563. https://doi.org/10.1038/372560a0

Evavold, C.L., J. Ruan, Y. Tan, S. Xia, H. Wu, and J.C. Kagan. 2018. The pore-forming protein gasdermin D regulates interleukin-1 secretion from living macrophages. *Immunity.* 48:35–44.e6. https://doi.org/10.1016/j.immuni.2017.11.013

Fahey, E., and S.L. Doyle. 2019. IL-1 family cytokine regulation of vascular permeability and angiogenesis. *Front. Immunol.* 10:1426. https://doi.org/10.3389/fimmu.2019.01426

Flynn, J.L., M.M. Goldstein, J. Chan, K.J. Triebold, K. Pfeffer, C.J. Lowenstein, R. Schreiber, T.W. Mak, and B.R. Bloom. 1995. Tumor necrosis factor-alpha is required in the protective immune response against Mycobacterium tuberculosis in mice. *Immunity.* 2:561–572. https://doi.org/10.1016/1074-7613(95)90001-2

Franchi, L., N. Kamada, Y. Nakamura, A. Burberry, P. Kuffa, S. Suzuki, M.H. Shaw, Y.G. Kim, and G. Núñez. 2012. NLRC4-driven production of IL-1β discriminates between pathogenic and commensal bacteria and promotes host intestinal defense. *Nat. Immunol.* 13:449–456. https://doi.org/10.1038/ni.2263

Gaidt, M.M., T.S. Ebert, D. Chauhan, T. Schmidt, J.L. Schmid-Burgk, F. Rapino, A.A. Robertson, M.A. Cooper, T. Graf, and V. Hornung. 2016. Human monocytes engage an alternative inflammasome pathway. *Immunity.* 44:833–846. https://doi.org/10.1016/j.immuni.2016.01.012

Galyov, E.E., S. Håkansson, A. Forsberg, and H. Wolf-Watz. 1993. A secreted protein kinase of Yersinia pseudotuberculosis is an indispensable virulence determinant. *Nature.* 361:730–732. https://doi.org/10.1038/361730a0

Glaccum, M.B., K.L. Stocking, K. Charrier, J.L. Smith, C.R. Willis, C. Maliszewski, D.J. Livingston, J.J. Peschon, and P.J. Morrissey. 1997. Phenotypic and functional characterization of mice that lack the type I receptor for IL-1. *J. Immunol.* 159:3364–3371. https://doi.org/10.4049/jimmunol.159.7.3364

Green, S.P., E.L. Hartland, R.M. Robins-Browne, and W.A. Phillips. 1995. Role of YopH in the suppression of tyrosine phosphorylation and respiratory burst activity in murine macrophages infected with Yersinia enterocolitica. *J. Leukoc. Biol.* 57:972–977. https://doi.org/10.1002/jlb.57.6.972

Greene, C.M., G. Meachery, C.C. Taggart, C.P. Rooney, R. Coakley, S.J. O'Neill, and N.G. McElvaney. 2000. Role of IL-18 in CD4⁺ T lymphocyte activation in sarcoidosis. *J. Immunol.* 165:4718–4724. https://doi.org/10.4049/jimmunol.165.8.4718

Grosdent, N., I. Maridonneau-Parini, M.P. Sory, and G.R. Cornelis. 2002. Role of Yops and adhesins in resistance of Yersinia enterocolitica to phagocytosis. *Infect. Immun.* 70:4165–4176. https://doi.org/10.1128/IAI.70.8.4165-4176.2002

Homaidan, F.R., G.S. Chakroun, W. Dbaibo, W. El-Assaad, and M.E. El-Sabban. 2001. IL-1 activates two phospholipid signaling pathways in intestinal epithelial cells. *Inflamm. Res.* 50:375–381. https://doi.org/10.1007/PL00000259

Horai, R., M. Asano, K. Sudo, H. Kanuka, M. Suzuki, M. Nishihara, M. Takahashi, and Y. Iwakura. 1998. Production of mice deficient in genes for

interleukin (IL)-1α, IL-1β, IL-1α/β, and IL-1 receptor antagonist shows that IL-1β is crucial in turpentine-induced fever development and glucocorticoid secretion. *J. Exp. Med.* 187:1463–1475. https://doi.org/10.1084/jem.187.9.1463

Hoshino, K., O. Takeuchi, T. Kawai, H. Sanjo, T. Ogawa, Y. Takeda, K. Takeda, and S. Akira. 1999. Cutting edge: Toll-like receptor 4 (TLR4)-deficient mice are hyporesponsive to lipopolysaccharide: Evidence for TLR4 as the Lps gene product. *J. Immunol.* 162:3749–3752. https://doi.org/10.4049/jimmunol.162.7.3749

Jain, A., R.A. Irizarry-Caro, M.M. McDaniel, A.S. Chawla, K.R. Carroll, G.R. Overcast, N.H. Philip, A. Oberst, A.V. Chervonsky, J.D. Katz, and C. Pasare. 2020. T cells instruct myeloid cells to produce inflammasome-independent IL-1β and cause autoimmunity. *Nat. Immunol.* 21:65–74. https://doi.org/10.1038/s41590-019-0559-y

Ji, D.X., L.H. Yamashiro, K.J. Chen, N. Mukaida, I. Kramnik, K.H. Darwin, and R.E. Vance. 2019. Type I interferon-driven susceptibility to Mycobacterium tuberculosis is mediated by IL-1Ra. *Nat. Microbiol.* 4:2128–2135. https://doi.org/10.1038/s41564-019-0578-3

Jung, C., U. Meinzer, N. Montcuquet, E. Thachil, D. Château, R. Thiébaut, M. Roy, Z. Alnabhani, D. Berrebi, M. Dussaillant, et al. 2012. Yersinia pseudotuberculosis disrupts intestinal barrier integrity through hematopoietic TLR-2 signaling. *J. Clin. Invest.* 122:2239–2251. https://doi.org/10.1172/JCI58147

Kindler, V., A.P. Sappino, G.E. Grau, P.F. Piguet, and P. Vassalli. 1989. The inducing role of tumor necrosis factor in the development of bactericidal granulomas during BCG infection. *Cell.* 56:731–740. https://doi.org/10.1016/0092-8674(89)90676-4

Kojima, M., Y. Morita, K. Shimizu, T. Yoshida, I. Yamada, T. Togo, and T. Johshita. 2007. Immunohistological findings of suppurative granulomas of Yersinia enterocolitica appendicitis: A report of two cases. *Pathol. Res. Pract.* 203:115–119. https://doi.org/10.1016/j.prp.2006.10.004

Kusnadi, A., S.H. Park, R. Yuan, T. Pannellini, E. Giannopoulou, D. Oliver, T. Lu, K.H. Park-Min, and L.B. Ivashkiv. 2019. The cytokine TNF promotes transcription factor SREBP activity and binding to inflammatory genes to activate macrophages and limit tissue repair. *Immunity.* 51:241–257.e9. https://doi.org/10.1016/j.immuni.2019.06.005

Lamps, L.W., K.T. Madhusudhan, J.K. Greenson, R.H. Pierce, N.A. Massoll, M.C. Chiles, P.J. Dean, and M.A. Scott. 2001. The role of Yersinia enterocolitica and Yersinia pseudotuberculosis in granulomatous appendicitis: A histologic and molecular study. *Am. J. Surg. Pathol.* 25:508–515. https://doi.org/10.1097/00000478-200104000-00011

Lee, Y.-S., H. Yang, J.Y. Yang, Y. Kim, S.H. Lee, J.H. Kim, Y.J. Jang, B.A. Vallance, and M.N. Kweon. 2015. Interleukin-1 (IL-1) signaling in intestinal stromal cells controls KC/CXCL1 secretion, which correlates with recruitment of IL-22- secreting neutrophils at early stages of Citrobacter rodentium infection. *Infect. Immun.* 83:3257–3267. https://doi.org/10.1128/IAI.00670-15

Lin, P.L., A. Myers, L. Smith, C. Bigbee, M. Bigbee, C. Fuhrman, H. Grieser, I. Chiosea, N.N. Voitenek, S.V. Capuano, et al. 2010. TNF neutralization results in disseminated disease during acute and latent *M. tuberculosis* infection with normal granuloma structure. *Arthritis Rheum.* 62:340–350. https://doi.org/10.1002/art.27271

Liu, X., M.A. Boyer, A.M. Holmgren, and S. Shin. 2020. Legionella-infected macrophages engage the alveolar epithelium to metabolically reprogram myeloid cells and promote antibacterial inflammation. *Cell Host Microbe.* 28:683–698.e6. https://doi.org/10.1016/j.chom.2020.07.019

Mann, B.S., and K.F. Chung. 2006. Blood neutrophil activation markers in severe asthma: Lack of inhibition by prednisolone therapy. *Respir. Res.* 7:59. https://doi.org/10.1186/1465-9921-7-59

Matty, M.A., F.J. Roca, M.R. Cronan, and D.M. Tobin. 2015. Adventures within the speckled band: Heterogeneity, angiogenesis, and balanced inflammation in the tuberculous granuloma. *Immunol. Rev.* 264:276–287. https://doi.org/10.1111/imr.12273

Mayer-Barber, K.D., D.L. Barber, K. Shenderov, S.D. White, M.S. Wilson, A. Cheever, D. Kugler, S. Hieny, P. Caspar, G. Núñez, et al. 2010. Caspase-1 independent IL-1β production is critical for host resistance to mycobacterium tuberculosis and does not require TLR signaling in vivo. *J. Immunol.* 184:3326–3330. https://doi.org/10.4049/jimmunol.0904189

Mayer-Barber, K.D., B.B. Andrade, D.L. Barber, S. Hieny, C.G. Feng, P. Caspar, S. Oland, S. Gordon, and A. Sher. 2011. Innate and adaptive interferons suppress IL-1α and IL-1β production by distinct pulmonary myeloid subsets during Mycobacterium tuberculosis infection. *Immunity.* 35:1023–1034. https://doi.org/10.1016/j.immuni.2011.12.002

Mecsas, J., B. Raupach, and S. Falkow. 1998. The Yersinia Yops inhibit invasion of Listeria, Shigella and Edwardsiella but not Salmonella into

epithelial cells. *Mol. Microbiol.* 28:1269–1281. https://doi.org/10.1046/j.1365-2958.1998.00891.x

Meinzer, U., F. Barreau, S. Esmiol-Welterlin, C. Jung, C. Villard, T. Léger, S. Ben-Mkaddem, D. Berrebi, M. Dussaillant, Z. Alnabhani, et al. 2012. Yersinia pseudotuberculosis effector YopJ subverts the Nod2/RICK/TAK1 pathway and activates caspase-1 to induce intestinal barrier dysfunction. *Cell Host Microbe.* 11:337–351. https://doi.org/10.1016/j.chom.2012.02.009

Monack, D.M., J. Mecsas, N. Ghori, and S. Falkow. 1997. Yersinia signals macrophages to undergo apoptosis and YopJ is necessary for this cell death. *Proc. Natl. Acad. Sci. USA.* 94:10385–10390. https://doi.org/10.1073/pnas.94.19.10385

Moon, C., K.L. VanDussen, H. Miyoshi, and T.S. Stappenbeck. 2014. Development of a primary mouse intestinal epithelial cell monolayer culture system to evaluate factors that modulate IgA transcytosis. *Mucosal Immunol.* 7:818–828. https://doi.org/10.1038/mi.2013.98

Mukherjee, S., G. Keitany, Y. Li, Y. Wang, H.L. Ball, E.J. Goldsmith, and K. Orth. 2006. Yersinia YopJ acetylates and inhibits kinase activation by blocking phosphorylation. *Science.* 312:1211–1214. https://doi.org/10.1126/science.1126867

Ofengeim, D., and J. Yuan. 2013. Regulation of RIP1 kinase signalling at the crossroads of inflammation and cell death. *Nat. Rev. Mol. Cell Biol.* 14:727–736. https://doi.org/10.1038/nrm3683

Orth, K., L.E. Palmer, Z.Q. Bao, S. Stewart, A.E. Rudolph, J.B. Bliska, and J.E. Dixon. 1999. Inhibition of the mitogen-activated protein kinase kinase superfamily by a Yersinia effector. *Science.* 285:1920–1923. https://doi.org/10.1126/science.285.5435.1920

Orzalli, M.H., A. Smith, K.A. Jurado, A. Iwasaki, J.A. Garlick, and J.C. Kagan. 2018. An antiviral branch of the IL-1 signaling pathway restricts immune-evasive virus replication. *Mol. Cell.* 71:825–840.e6. https://doi.org/10.1016/j.molcel.2018.07.009

Overcast, G.R., H.E. Meibers, E.M. Eshleman, I. Saha, L. Waggoner, K.N. Patel, V.G. Jain, D.B. Haslam, T. Alenghat, K.L. VanDussen, and C. Pasare. 2023. IEC-intrinsic IL-1R signaling holds dual roles in regulating intestinal homeostasis and inflammation. *J. Exp. Med.* 220:e20212523. https://doi.org/10.1084/jem.20212523

Pagán, A.J., and L. Ramakrishnan. 2018. The Formation and function of granulomas. *Annu. Rev. Immunol.* 36:639–665. https://doi.org/10.1146/annurev-immunol-032712-100022

Palmer, L.E., S. Hobbie, J.E. Galán, and J.B. Bliska. 1998. YopJ of Yersinia pseudotuberculosis is required for the inhibition of macrophage TNF-α production and downregulation of the MAP kinases p38 and JNK. *Mol. Microbiol.* 27:953–965. https://doi.org/10.1046/j.1365-2958.1998.00740.x

Di Paolo, N.C., S. Shafiani, T. Day, T. Papayannopoulou, D.W. Russell, Y. Iwakura, D. Sherman, K. Urdahl, and D.M. Shayakhmetov. 2015. Interdependence between interleukin-1 and tumor necrosis factor regulates TNF-dependent control of Mycobacterium tuberculosis infection. *Immunity.* 43:1125–1136. https://doi.org/10.1016/j.immuni.2015.11.016

Parent, M.A., L.B. Wilhelm, L.W. Kummer, F.M. Szaba, I.K. Mullarky, and S.T. Smiley. 2006. Gamma interferon, tumor necrosis factor alpha, and nitric oxide synthase 2, key elements of cellular immunity, perform critical protective functions during humoral defense against lethal pulmonary Yersinia pestis infection. *Infect. Immun.* 74:3381–3386. https://doi.org/10.1128/IAI.00185-06

Petersen, H.J. and A.M. Smith. 2013. The role of the innate immune system in granulomatous disorders. *Front. Immunol.* 4:120. https://doi.org/10.3389/fimmu.2013.00120

Peterson, L.W., N.H. Philip, C.P. Dillon, J. Bertin, P.J. Gough, D.R. Green, and I.E. Brodsky. 2016. Cell-extrinsic TNF collaborates with TRIF signaling to promote yersinia-induced apoptosis. *J. Immunol.* 197:4110–4117. https://doi.org/10.4049/jimmunol.1601294

Peterson, L.W., N.H. Philip, A. DeLaney, M.A. Wynosky-Dolfi, K. Asklof, F. Gray, R. Choa, E. Bjanes, E.L. Buza, R. Hu, et al. 2017. RIPK1-dependent apoptosis bypasses pathogen blockade of innate signaling to promote immune defense. *J. Exp. Med.* 214:3171–3182. https://doi.org/10.1084/jem.20170347

Pfeffer, K., T. Matsuyama, T.M. Kündig, A. Wakeham, K. Kishihara, A. Shahinian, K. Wiegmann, P.S. Ohashi, M. Krönke, and T.W. Mak. 1993. Mice deficient for the 55 kd tumor necrosis factor receptor are resistant to endotoxic shock, yet succumb to L. monocytogenes infection. *Cell.* 73:457–467. https://doi.org/10.1016/0092-8674(93)90134-C

Pham, T.H.M., S.M. Brewer, T. Thurston, L.M. Massis, J. Honeycutt, K. Lugo, A.R. Jacobson, J.G. Vilches-Moure, M. Hamblin, S. Helaine, and D.M. Monack. 2020. Salmonella-driven polarization of granuloma

macrophages antagonizes TNF-mediated pathogen restriction during persistent infection. *Cell Host Microbe*. 27:54–67.e5. https://doi.org/10.1016/j.chom.2019.11.011

Philip, N.H., C.P. Dillon, A.G. Snyder, P. Fitzgerald, M.A. Wynosky-Dolfi, E.E. Zwack, B. Hu, L. Fitzgerald, E.A. Mauldin, A.M. Copenhaver, et al. 2014. Caspase-8 mediates caspase-1 processing and innate immune defense in response to bacterial blockade of NF-κB and MAPK signaling. *Proc. Natl. Acad. Sci. USA*. 111:7385–7390. https://doi.org/10.1073/pnas.1403252111

Raskin, R.E. 2010. General Categories of Cytologic Interpretation. *In* Canine and Feline Cytology: A Color Atlas and Interpretation Guide. W.B. Saunders, editor. Second edition. Elsevier, St. Louis, MO. pp. 15–25. 10.1016/B978-141604985-2.50001-3.

Ratner, D., M.P. Orning, K.K. Starheim, R. Marty-Roix, M.K. Proulx, J.D. Goguen, and E. Lien. 2016. Manipulation of interleukin-1β and interleukin-18 production by yersinia pestis effectors YopJ and YopM and redundant impact on virulence. *J. Biol. Chem.* 291:9894–9905. https://doi.org/10.1074/jbc.M115.697698

Richardson, T., M. Jones, Y. Akhtar, and J. Pollard. 2018. Suspicious Yersinia granulomatous enterocolitis mimicking appendicitis. *BMJ Case Rep.* 2018:bcr2018224177. https://doi.org/10.1136/bcr-2018-224177

Roach, D.R., A.G. Bean, C. Demangel, M.P. France, H. Briscoe, and W.J. Britton. 2002. TNF regulates chemokine induction essential for cell recruitment, granuloma formation, and clearance of mycobacterial infection. *J. Immunol.* 168:4620–4627. https://doi.org/10.4049/jimmunol.168.9.4620

Rohena, F.J., M.I. Almira-Suárez, and C. González-Keelan. 2014. Granulomatous enterocolitis secondary to Yersinia in an 11-year-old boy from Puerto Rico, confirmed by PCR: A case report. *P. R. Health Sci. J.* 33: 27–30.

Rosqvist, R., I. Bölin, and H. Wolf-Watz. 1988. Inhibition of phagocytosis in Yersinia pseudotuberculosis: A virulence plasmid-encoded ability involving the Yop2b protein. *Infect. Immun.* 56:2139–2143. https://doi.org/10.1128/iai.56.8.2139-2143.1988

Rosqvist, R., A. Forsberg, and H. Wolf-Watz. 1991. Intracellular targeting of the Yersinia YopE cytotoxin in mammalian cells induces actin microfilament disruption. *Infect. Immun.* 59:4562–4569. https://doi.org/10.1128/iai.59.12.4562-4569.1991

Satpathy, A.T., C.G. Briseño, J.S. Lee, D. Ng, N.A. Manieri, W. Kc, X. Wu, S.R. Thomas, W.L. Lee, M. Turkoz, et al. 2013. Notch2-dependent classical dendritic cells orchestrate intestinal immunity to attaching-and-effacing bacterial pathogens. *Nat. Immunol.* 14:937–948. https://doi.org/10.1038/ni.2679

Scarpa, M., S. Kessler, T. Sadler, G. West, C. Homer, C. McDonald, C. de la Motte, C. Fiocchi, and E. Stylianou. 2015. The epithelial danger signal IL-1α is a potent activator of fibroblasts and reactivator of intestinal inflammation. *Am. J. Pathol.* 185:1624–1637. https://doi.org/10.1016/j.ajpath.2015.02.018

Serbina, N.V., and E.G. Pamer. 2006. Monocyte emigration from bone marrow during bacterial infection requires signals mediated by chemokine receptor CCR2. *Nat. Immunol.* 7:311–317. https://doi.org/10.1038/ni1309

Silvério, D., R. Gonçalves, R. Appelberg, and M. Saraiva. 2021. Advances on the role and applications of interleukin-1 in tuberculosis. *MBio.* 12: e0313421. https://doi.org/10.1128/mBio.03134-21

Simonet, M., and S. Falkow. 1992. Invasin expression in Yersinia pseudotuberculosis. *Infect. Immun.* 60:4414–4417. https://doi.org/10.1128/iai.60.10.4414-4417.1992

Sorobetea, D., R. Matsuda, S.T. Peterson, J.P. Grayczyk, I. Rao, E. Krespan, M. Lanza, C.A. Assenmacher, M. Mack, D.P. Beiting, et al. 2023.

Inflammatory monocytes promote granuloma control of Yersinia infection. *Nat. Microbiol.* 8:666–678. https://doi.org/10.1038/s41564-023-01338-6

Sugawara, I., H. Yamada, S. Hua, and S. Mizuno. 2001. Role of interleukin (IL)-1 type 1 receptor in mycobacterial infection. *Microbiol. Immunol.* 45: 743–750. https://doi.org/10.1111/j.1348-0421.2001.tb01310.x

Taheri, N., A. Fahlgren, and M. Fällman. 2016. Yersinia pseudotuberculosis blocks neutrophil degranulation. *Infect. Immun.* 84:3369–3378. https://doi.org/10.1128/IAI.00760-16

Takeda, K., and S. Akira. 2004. TLR signaling pathways. *Semin. Immunol.* 16: 3–9. https://doi.org/10.1016/j.smim.2003.10.003

Tobin, D.M., J.C. Vary Jr., J.P. Ray, G.S. Walsh, S.J. Dunstan, N.D. Bang, D.A. Hagge, S. Khadge, M.C. King, T.R. Hawn, et al. 2010. The lta4h locus modulates susceptibility to mycobacterial infection in zebrafish and humans. *Cell.* 140:717–730. https://doi.org/10.1016/j.cell.2010.02.013

Tobin, D.M., F.J. Roca, S.F. Oh, R. McFarland, T.W. Vickery, J.P. Ray, D.C. Ko, Y. Zou, N.D. Bang, T.T. Chau, et al. 2012. Host genotype-specific therapies can optimize the inflammatory response to mycobacterial infections. *Cell.* 148:434–446. https://doi.org/10.1016/j.cell.2011.12.023

Townsend, M.J., P.G. Fallon, D.J. Matthews, H.E. Jolin, and A.N. McKenzie. 2000. T1/ST2-deficient mice demonstrate the importance of T1/ST2 in developing primary T helper cell type 2 responses. *J. Exp. Med.* 191: 1069–1076. https://doi.org/10.1084/jem.191.6.1069

Vladimer, G.I., D. Weng, S.W. Paquette, S.K. Vanaja, V.A. Rathinam, M.H. Aune, J.E. Conlon, J.J. Burbage, M.K. Proulx, Q. Liu, et al. 2012. The NLRP12 inflammasome recognizes Yersinia pestis. *Immunity.* 37:96–107. https://doi.org/10.1016/j.immuni.2012.07.006

Weinlich, R., and D.R. Green. 2014. The two faces of receptor interacting protein kinase-1. *Mol. Cell.* 56:469–480. https://doi.org/10.1016/j.molcel.2014.11.001

Yamada, H., S. Mizumo, R. Horai, Y. Iwakura, and I. Sugawara. 2000. Protective role of interleukin-1 in mycobacterial infection in IL-1 α/β double-knockout mice. *Lab. Invest.* 80:759–767. https://doi.org/10.1038/labinvest.3780079

Yan, S.R., R.R. Joseph, J. Wang, and A.W. Stadnyk. 2006. Differential pattern of inflammatory molecule regulation in intestinal epithelial cells stimulated with IL-1. *J. Immunol.* 177:5604–5611. https://doi.org/10.4049/jimmunol.177.8.5604

Yeap, H.W., and K.W. Chen. 2022. RIPK1 and RIPK3 in antibacterial defence. *Biochem. Soc. Trans.* 50:1583–1594. https://doi.org/10.1042/BST20211242

Yoon, J.W., M.V. Pahl, and N.D. Vaziri. 2007. Spontaneous leukocyte activation and oxygen-free radical generation in end-stage renal disease. *Kidney Int.* 71:167–172. https://doi.org/10.1038/sj.ki.5002019

Yoon, S., Z. Liu, Y. Eyobo, and K. Orth. 2003. Yersinia effector YopJ inhibits yeast MAPK signaling pathways by an evolutionarily conserved mechanism. *J. Biol. Chem.* 278:2131–2135. https://doi.org/10.1074/jbc.M209905200

Zhang, Y., C. Khairallah, B.S. Sheridan, A.W.M. van der Velden, and J.B. Bliska. 2018. CCR2⁺ inflammatory monocytes are recruited to Yersinia pseudotuberculosis pyogranulomas and dictate adaptive responses at the expense of innate immunity during oral infection. *Infect. Immun.* 86: e00782-17. https://doi.org/10.1128/IAI.00782-17

Zhivaki, D., F. Borriello, O.A. Chow, B. Doran, I. Fleming, D.J. Theisen, P. Pallis, A.K. Shalek, C.L. Sokol, I. Zanoni, and J.C. Kagan. 2020. Inflammasomes within hyperactive murine dendritic cells stimulate long-lived T cell-mediated anti-tumor immunity. *Cell Rep.* 33:108381. https://doi.org/10.1016/j.celrep.2020.108381
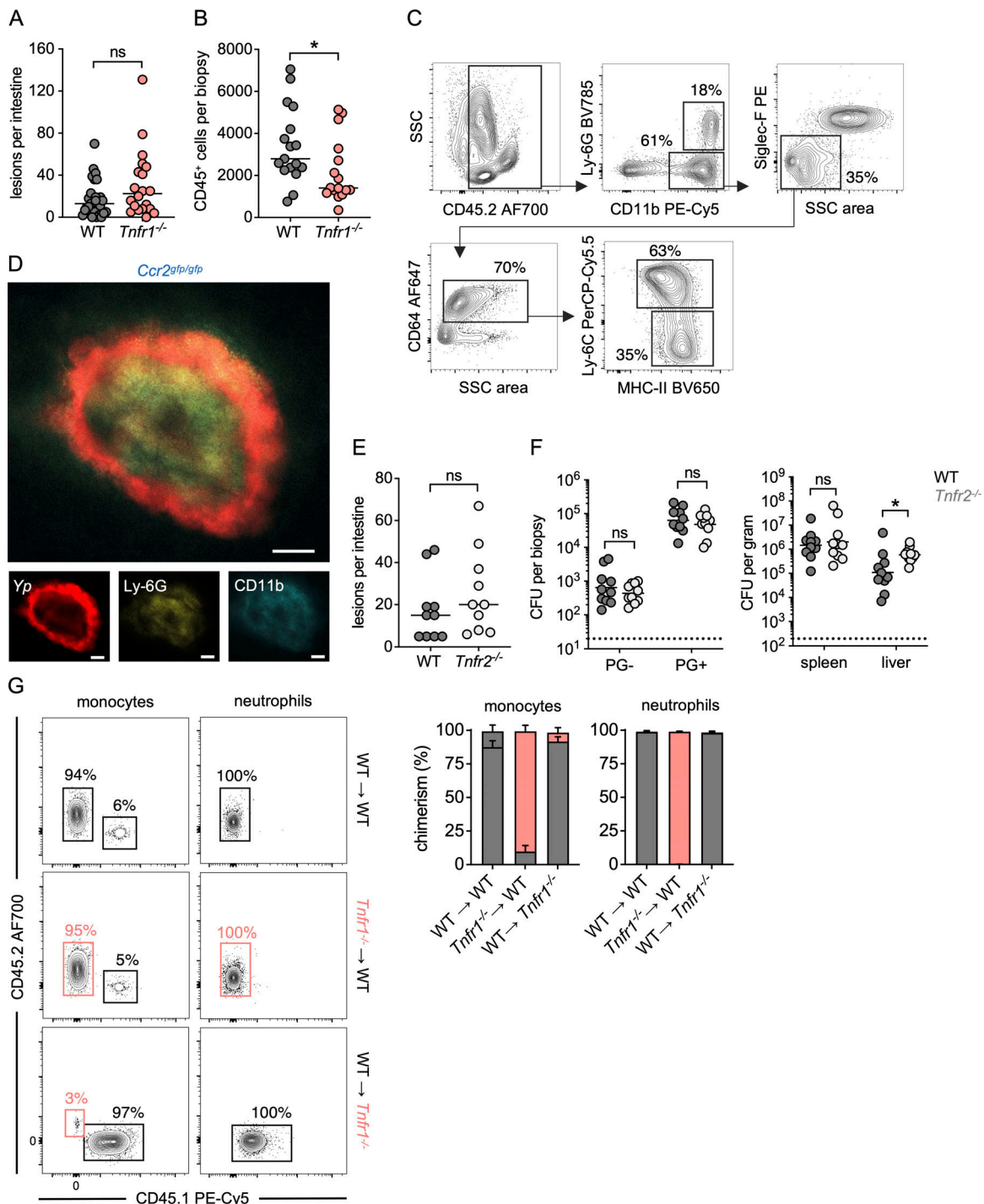
Supplemental material

Figure S1. **Effects of TNFR1 deficiency on PG formation in intestinal and lymphatic tissue during *Yp* infection. (A)** Total number of intestinal lesions at day 5 after infection with *Yp*. Each circle represents one mouse. Lines represent the median. Pooled data from four independent experiments. **(B)** Total numbers of CD45+ hematopoietic cells in PG+ small intestinal tissue isolated 5 days after infection. Each circle represents the mean of 3–20 pooled punch biopsies from one mouse. Lines represent the median. Pooled data from three independent experiments. **(C)** Flow cytometry plots depicting the gating strategy employed to identify neutrophils (CD11b+ Ly-6G+), monocytes (CD64+ Ly-6C^{hi}), and macrophages (CD64+ Ly-6C^{lo} MHC-II^{hi}) in small intestinal PG+ tissue. Plots representative of three independent experiments. **(D)** Fluorescently labeled whole-mount small intestinal PG+ tissue from *Yp*-infected *Ccr2$^{gfp/gfp}$* mouse at day 5 after infection. Red (*Yp*-mCherry), yellow (Ly-6G-AF647), and blue (CD11b-AF700). Scale bar = 100 μm. Representative image of two independent experiments. **(E)** Total number of intestinal lesions at day 5 after infection with *Yp*. Each circle represents one mouse. Lines represent the median. Pooled data from two independent experiments. **(F)** Bacterial burdens in small intestinal PG− and PG+ tissue (left) and indicated organs (right) isolated day 5 after infection. Each circle represents the mean CFU of three to five pooled punch biopsies from one mouse (left) or individual mice (right). Lines represent the geometric mean. Pooled data from two independent experiments. **(G)** Flow cytometry plots depicting chimerism (left) and frequencies of indicated cell types (right) in the blood of uninfected chimeric mice. Graphs represent pooled data from two independent experiments. All statistical analyses by Mann–Whitney U test. *P < 0.05, ns = not significant.
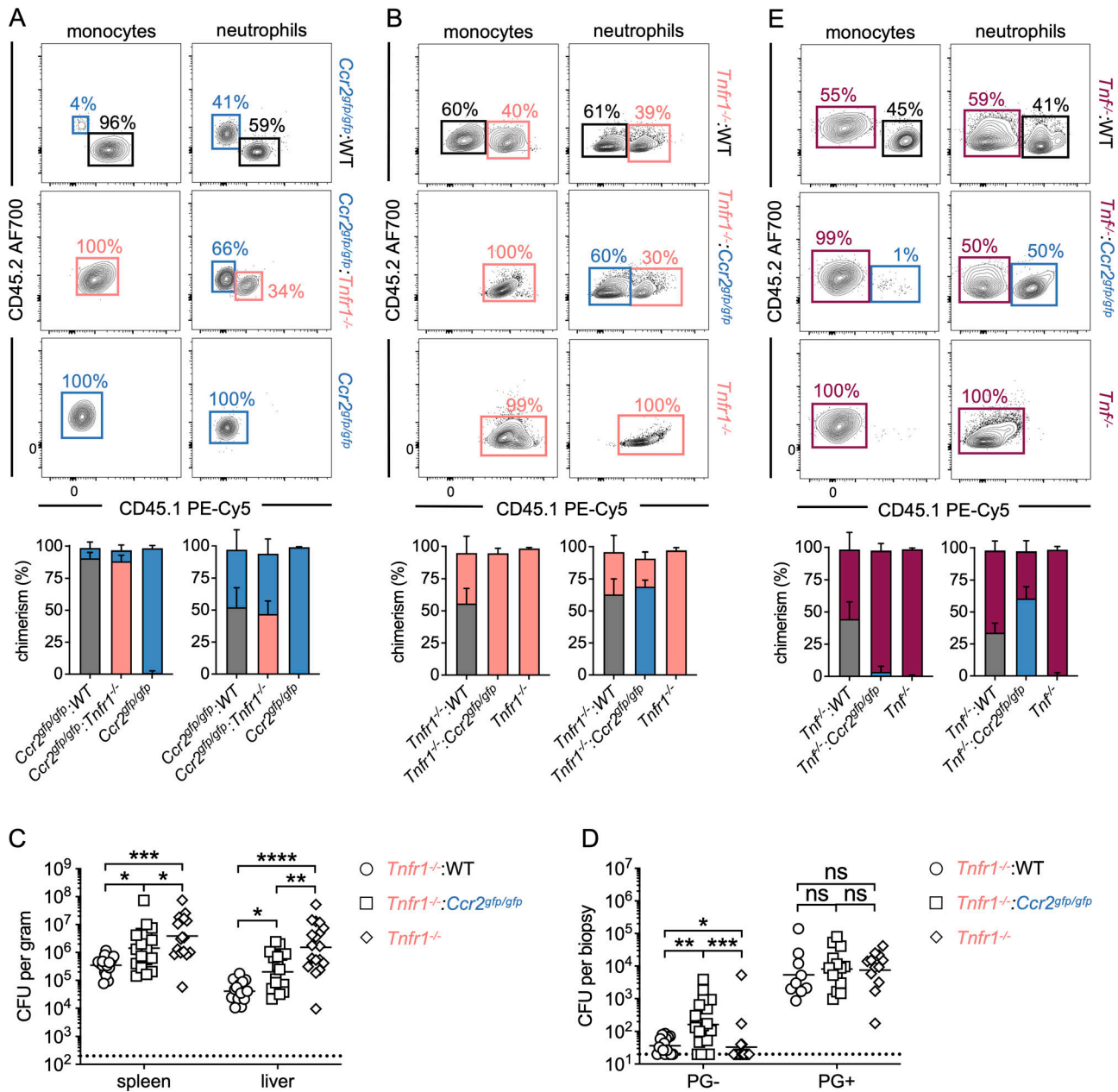
Figure S2. **Autocrine TNF signaling in monocytes is required for systemic control of *Yp*. (A)** Flow cytometry plots (top) and graphs (bottom) depicting the percent chimerism of hematopoietic cells in the blood of uninfected chimeric mice. **(B)** Flow cytometry plots (top) and graphs (bottom) depicting the percent chimerism of hematopoietic cells in the spleens of chimeric mice. **(C)** Bacterial burdens in indicated organs at day 5 after infection. Each symbol represents one mouse. Lines represent the geometric mean. **(D)** Bacterial burdens in small intestinal PG⁻ and PG⁺ tissue at day 5 after *Yp* infection. Each symbol represents one mouse. Lines represent the geometric mean. **(E)** Flow cytometry plots (top) and graphs (bottom) depicting the percent chimerism of hematopoietic cells in PG of chimeric mice. All data were pooled from two independent experiments. All statistical analyses by Kruskal–Wallis test with Dunn's multiple comparisons correction. *P < 0.05, **P < 0.01, ***P < 0.001, ****P < 0.0001, ns = not significant.
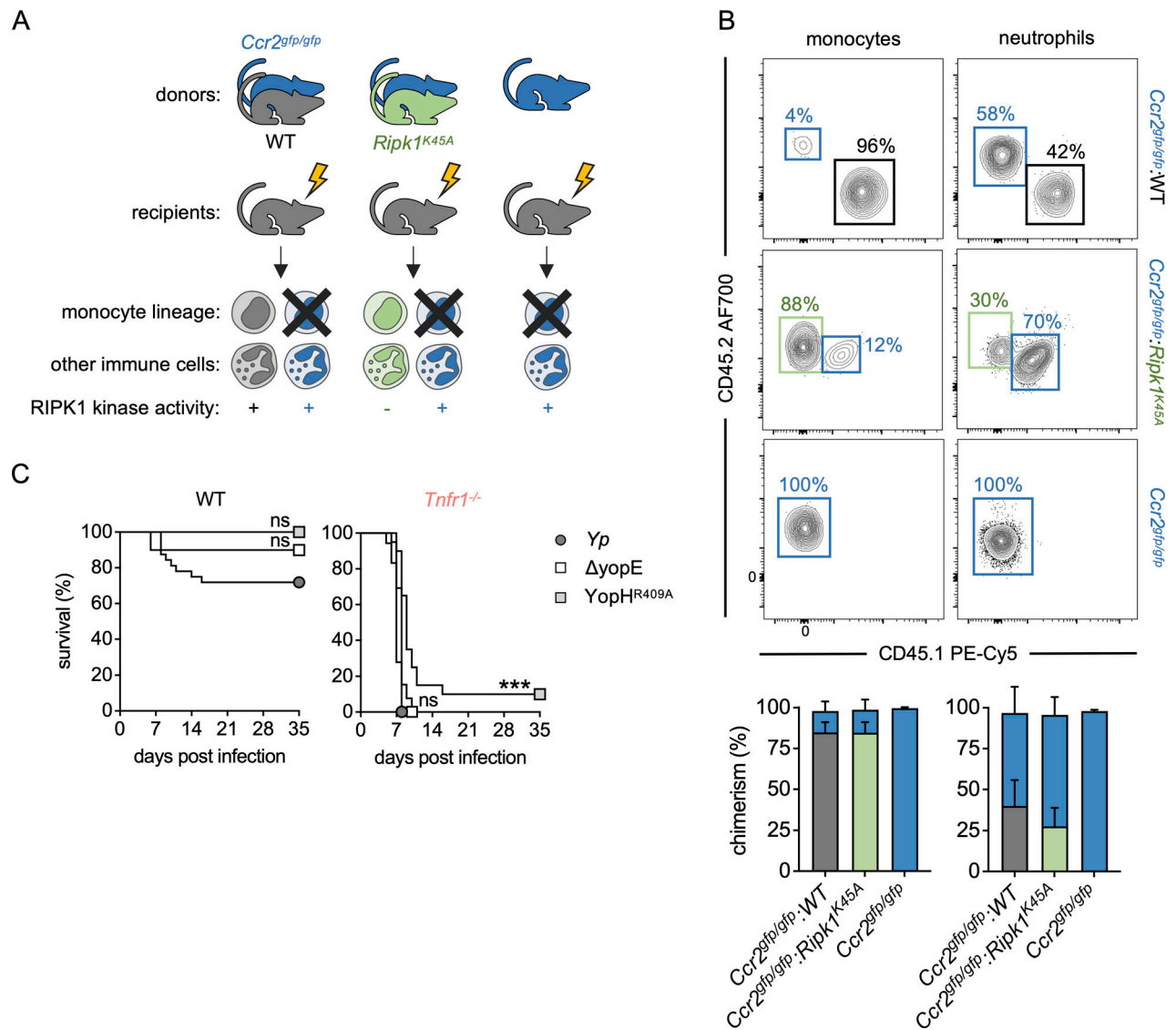
Figure S3. **TNFR1 signaling in monocytes is independent of YopJ-induced RIPK1 kinase activity. (A)** Schematic of mixed BM chimeras. Lethally irradiated WT mice reconstituted with BM cells from indicated donor mice yield either a RIPK1 kinase–sufficient immune system (left), one in which all monocytes lack RIPK1 kinase activity whereas half of the remaining immune cells are RIPK1 kinase–sufficient (middle), or a RIPK1 kinase–sufficient immune system devoid of monocytes (right). **(B)** Flow cytometry plots depicting chimerism (top) and graphs depicting frequencies of indicated cell types (bottom) in the blood of uninfected chimeric mice. **(C)** Survival of WT (left) and $Tnfr1^{-/-}$ (right) mice infected with WT (circles), $\Delta yopE$ (white squares), or YopH^{R409A} (gray squares) Yp. n = 5–32 (WT) and 13–20 ($Tnfr1^{-/-}$) mice per group. Pooled data from two to four independent experiments. All statistical analyses by Mantel–Cox test. ***P < 0.001, ns = not significant.
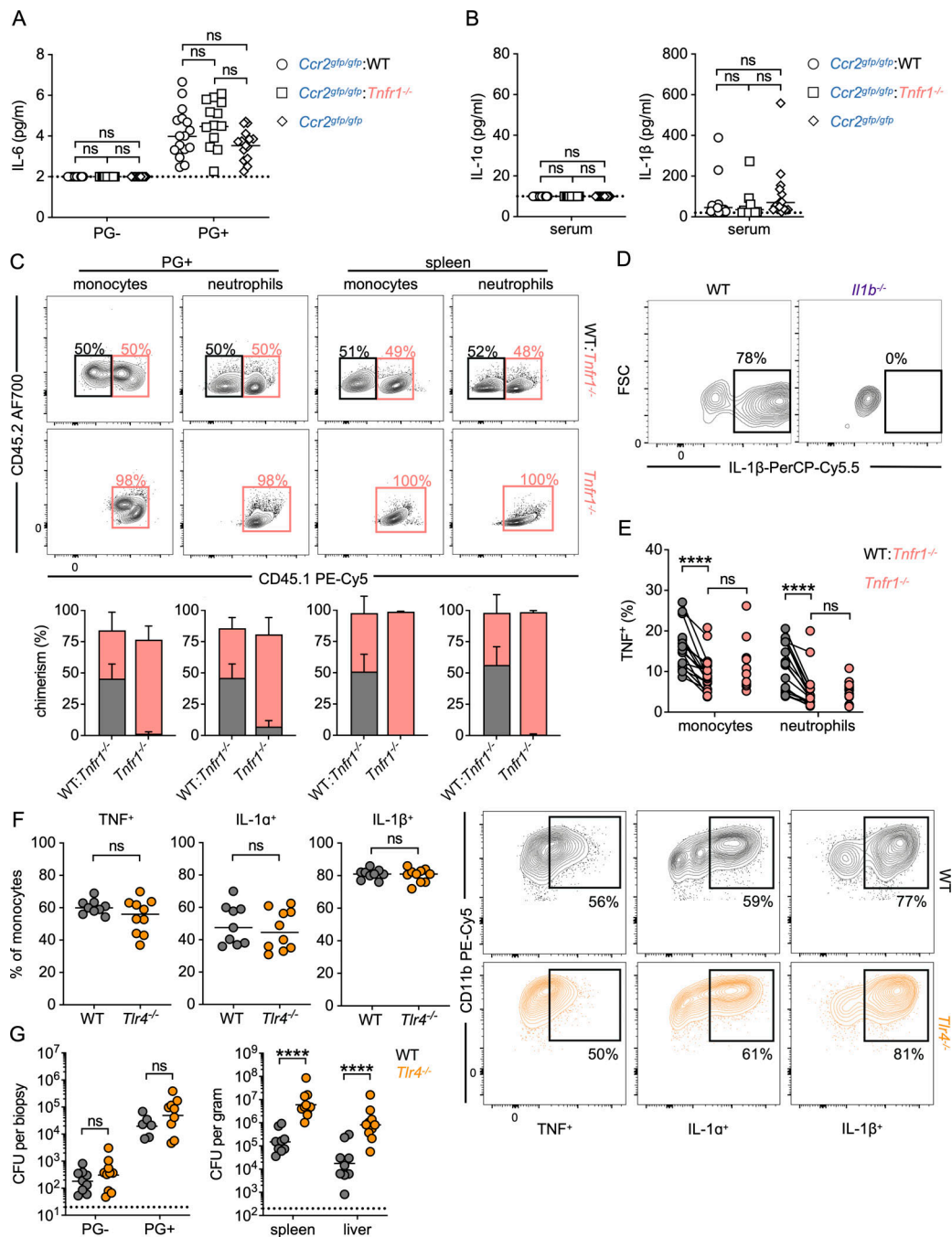
Figure S4. **Cytokine production downstream of TNFR1 expression on monocytes is specific to IL-1 in intestinal PGs. (A)** Cytokine levels in homogenates of PG− and PG+ tissue punch biopsies at day 5 after infection of chimeric WT mice reconstituted with indicated cells. Each symbol represents the mean of 3–10 pooled punch biopsies from one mouse. Lines represent the median. Pooled data from two independent experiments. **(B)** Cytokine levels in serum at day 5 after infection of chimeric WT mice reconstituted with indicated cells. Lines represent the median. Pooled data from two independent experiments. **(C)** Flow cytometric plots and graphs depicting frequencies of indicated cell types in small intestinal PG+ tissue or spleen at day 5 after infection of WT chimeric mice reconstituted with the indicated cells. Plots representative of two independent experiments. Pooled data from two independent experiments. **(D)** Flow cytometry plots of intracellular IL-1 in monocytes (CD64+ Ly-6C^{hi}) from small intestinal PG+ tissue in WT and *Il1b*$^{−/−}$ mice at day 5 after infection. Plots representative of two independent experiments. **(E)** Frequency of monocytes and neutrophils producing TNF in small intestinal PG+ tissue at day 5 after infection. Each circle represents the mean of 3–10 pooled punch biopsies from one mouse. Lines connect congenic cell populations within individual mice. Pooled data from two independent experiments. **(F)** Frequency of monocytes producing the indicated cytokines (left) and flow cytometric plots depicting intracellular cytokine staining (right) in monocytes isolated from small intestinal PG+ tissue 5 days after infection. Each circle represents the mean of 3–10 pooled punch biopsies from one mouse. Lines represent the median. Pooled data from three independent experiments. **(G)** Bacterial burdens in small intestinal PG− and PG+ tissue (left) and indicated organs (right) of WT and *Tlr4*$^{−/−}$ mice at day 5 after *Yp* infection. Each symbol represents one mouse. Lines represent the geometric mean. Pooled data from two independent experiments. Statistical analyses by Kruskal–Wallis test with Dunn's multiple comparisons correction (A and B). For congenically marked cells within mice, Wilcoxon test; across groups, Mann–Whitney U test (E), and Mann–Whitney U test (F and G). ****P < 0.0001, ns = not significant.
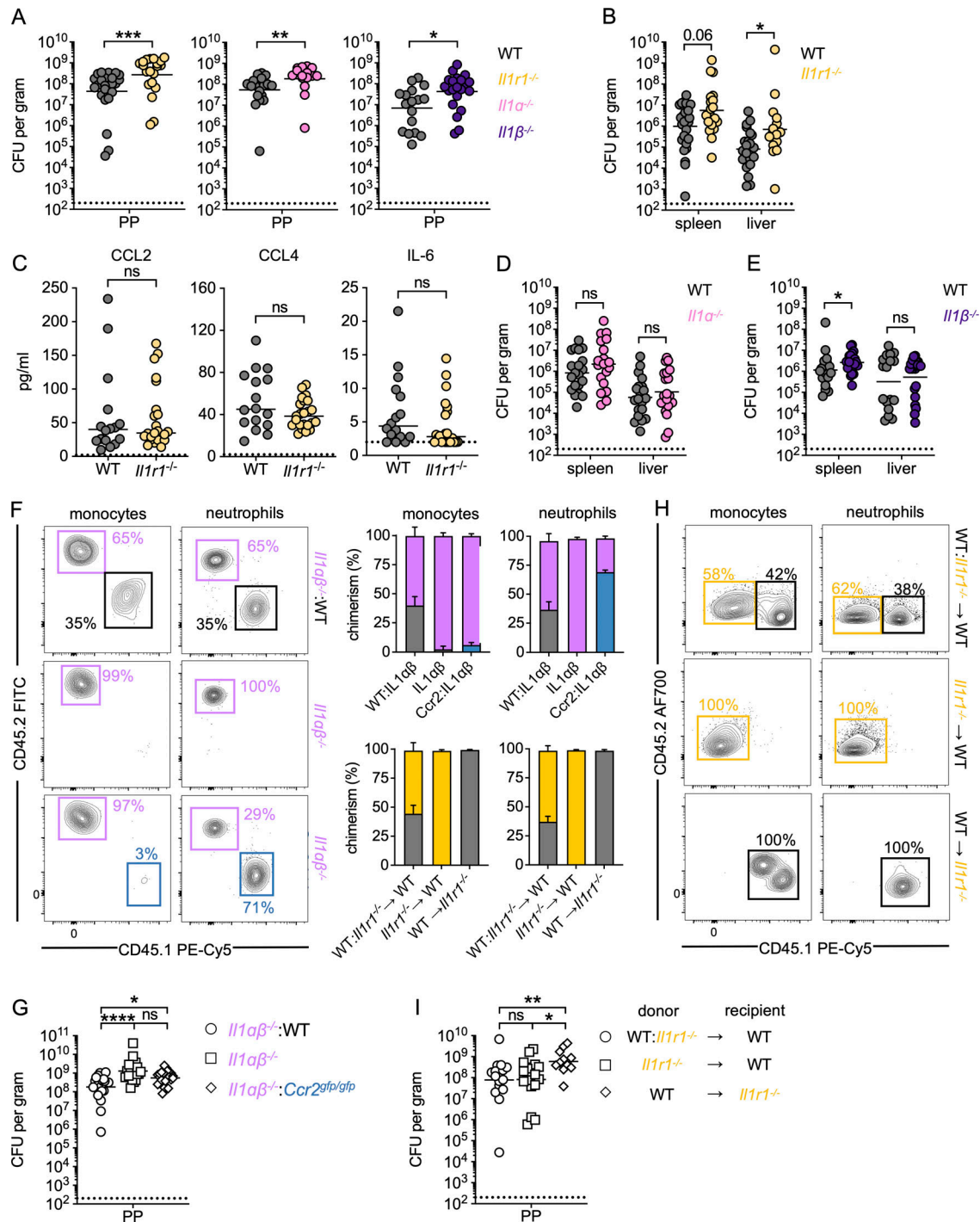
Figure S5. **Monocyte-derived IL-1 signals to non-hematopoietic cells to restrict *Yp* infection. (A)** Bacterial burdens in Peyer's patches (PP) at day 5 after infection. Each circle represents one mouse. Lines represent the geometric mean. Pooled data from three independent experiments. **(B)** Bacterial burdens in indicated organs at day 5 after infection. Each circle represents one mouse. Lines represent the geometric mean. Pooled data from three independent experiments. **(C)** Cytokine levels in PG+ tissue punch biopsy homogenates isolated 5 days after infection. Each datapoint represents the mean of 3–20 pooled bunch biopsies from one mouse. Lines represent the median. Pooled data from three independent experiments. **(D and E)** Bacterial burdens in indicated organs at day 5 after infection. Each circle represents one mouse. Lines represent the geometric mean. Pooled data from three independent experiments. **(F)** Flow cytometric plots and graphs depicting the percent chimerism in the blood of chimeric mice. Flow cytometric plots are representative of two independent experiments. Pooled data from two independent experiments. **(G)** Bacterial burdens in Peyer's patches isolated 5 days after infection. Each symbol represents one mouse. Lines represent the geometric mean. Pooled data from three independent experiments. **(H)** Frequencies of indicated cell types in small intestinal PG+ tissue at day 5 after infection of indicated chimeric mouse. Pooled data from three independent experiments. **(I)** Bacterial burdens in Peyer's patches isolated 5 days after infection. Each symbol represents one mouse. Lines represent the geometric mean. Pooled data from three independent experiments. Statistical analysis by Mann–Whitney U test (A–E), and Kruskal–Wallis test with Dunn's multiple comparisons correction (G and I). *P < 0.05, **P < 0.01, ***P < 0.001, ****P < 0.0001, ns = not significant.